

4

DTIC FILE COPY

TECHNICAL REPORT BRL-TR-3054

BRL

THE PENETRATION OF FRAGMENTS
INTO COLLECTION MEDIA

HUBERT W. MEYER, JR.
FRED I. GRACE

~~DECEMBER~~ 1989

DTIC
ELECTE
OCT. 31 1989
S B D
CO

APPROVED FOR PUBLIC RELEASE; DISTRIBUTION UNLIMITED.

U.S. ARMY LABORATORY COMMAND

BALLISTIC RESEARCH LABORATORY
ABERDEEN PROVING GROUND, MARYLAND

AD-A213 878

89 10 30 233

DESTRUCTION NOTICE

Destroy this report when it is no longer needed. DO NOT return it to the originator.

Additional copies of this report may be obtained from the National Technical Information Service, U.S. Department of Commerce, Springfield, VA 22161.

The findings of this report are not to be construed as an official Department of the Army position, unless so designated by other authorized documents.

The use of trade names or manufacturers' names in this report does not constitute indorsement of any commercial product.

REPORT DOCUMENTATION PAGE

Form Approved
OMB No. 0704-0188

1a. REPORT SECURITY CLASSIFICATION Unclassified		1b. RESTRICTIVE MARKINGS	
2a. SECURITY CLASSIFICATION AUTHORITY		3. DISTRIBUTION/AVAILABILITY OF REPORT Approved for public release; Unlimited Distribution	
2b. DECLASSIFICATION/DOWNGRADING SCHEDULE			
4. PERFORMING ORGANIZATION REPORT NUMBER(S) BRL-TR-3054		5. MONITORING ORGANIZATION REPORT NUMBER(S)	
6a. NAME OF PERFORMING ORGANIZATION Ballistic Research Laboratory	6b. OFFICE SYMBOL (If applicable) SLCBR-TB-AA	7a. NAME OF MONITORING ORGANIZATION	
6c. ADDRESS (City, State, and ZIP Code) Aberdeen Proving Ground, MD 21005-5066		7b. ADDRESS (City, State, and ZIP Code)	
8a. NAME OF FUNDING/SPONSORING ORGANIZATION	8b. OFFICE SYMBOL (If applicable)	9. PROCUREMENT INSTRUMENT IDENTIFICATION NUMBER	
8c. ADDRESS (City, State, and ZIP Code)		10. SOURCE OF FUNDING NUMBERS	
		PROGRAM ELEMENT NO.	PROJECT NO.
		TASK NO.	WORK UNIT ACCESSION NO.
11. TITLE (Include Security Classification) The Penetration of Fragments into Collection Media			
12. PERSONAL AUTHOR(S) Hubert W. Meyer, Jr., Fred I. Grace			
13a. TYPE OF REPORT Technical	13b. TIME COVERED FROM _____ TO _____	14. DATE OF REPORT (Year, Month, Day)	15. PAGE COUNT
16. SUPPLEMENTARY NOTATION			
17. COSATI CODES		18. SUBJECT TERMS (Continue on reverse if necessary and identify by block number)	
FIELD	GROUP	SUB-GROUP	
		Fragments, Ammunition, Penetration, Collection Media, (JIS)	
19. ABSTRACT (Continue on reverse if necessary and identify by block number) A generalized resistive force law is proposed to describe the penetration of fragments into collection media. An empirical model for predicting fragment striking velocity is obtained from the assumed force law. Three successive simplifications of the model are studied and their accuracies compared. The familiar $V = KM^A P^B A^C$ expression is obtained from the model and explicit relations among the exponents are revealed. The usefulness of these relations is demonstrated. The concept of homologous fragment sets, wherein $A = kM^2$, is discussed.			
20. DISTRIBUTION/AVAILABILITY OF ABSTRACT <input checked="" type="checkbox"/> UNCLASSIFIED/UNLIMITED <input type="checkbox"/> SAME AS RPT. <input type="checkbox"/> DTIC USERS		21. ABSTRACT SECURITY CLASSIFICATION UNCLASSIFIED	
22a. NAME OF RESPONSIBLE INDIVIDUAL Hubert W. Meyer, Jr.		22b. TELEPHONE (Include Area Code) 301-278-6019	22c. OFFICE SYMBOL SLCBR-TB-AA

TABLE OF CONTENTS

	PAGE
LIST OF TABLES	v
LIST OF ILLUSTRATIONS	vii
I. INTRODUCTION	1
II. THE MODEL	2
III. APPLICATION OF THE MODEL: METHOD I	4
IV. SIMPLIFYING THE MODEL	11
V. COMPARISON TO EXISTING CALIBRATION EXPRESSIONS	15
VI. APPLICATIONS OF THE SIMPLIFIED MODEL	16
A. CALIBRATION	16
B. METHOD II	20
C. METHOD III	24
D. METHOD IV	28
VII. CONCLUSIONS	31
REFERENCES	35
APPENDIX	37
DISTRIBUTION LIST	49



Accession For	
NTIS GRA&I	<input checked="" type="checkbox"/>
DTIC TAB	<input type="checkbox"/>
Unannounced	<input type="checkbox"/>
Justification	
By _____	
Distribution/	
Availability Codes	
Dist	Avail and/or Special
A-1	

LIST OF TABLES

TABLE	PAGE
1. Computation of Impact medium Calibration Constant c	8
2. Numerical Integration of the Integral	9
3. Evaluation of Equations 28 and 29 by Empirically Determined Constants	17
4. Variation with Fragment Mass of Calibration Constants β and b_1	20
5. Summary of Methods	33
A-1. Calibration of Impact Medium using 57 mg Steel Spheres	39
A-2. Small Fragment Data: $36\text{mg} \leq m \leq 80\text{mg}$	40
A-3. Calibration of Impact Medium using 700mg Steel Spheres	42
A-4. Calibration of Impact Medium using 1025mg Steel Spheres	43
A-5. Calibration of Impact Medium using 1002mg to 1059 mg Steel Spheres.	44
A-6. Fragment Area and Mass Data	45

LIST OF ILLUSTRATIONS

FIGURE		PAGE
1.	Parametric Variation of Calibration Data	7
2.	Approximation of the Integral	10
3.	Results of Method I	12
4.	Fragment penetration as a Function of Instantaneous Fragment Velocity	14
5.	Sphere Calibration of Impact Medium Using 57mg Spheres	21
6.	Sphere Calibration of Impact Medium Using 700mg Spheres	22
7.	Sphere Calibration of Impact Medium Using 1025mg Spheres	23
8.	Results of Method II	25
9.	Relationship between Fragment Area and Fragment Mass for the Entire Fragment Population	27
10.	Results of Method III	29
11.	Results of Method IV	32

I. INTRODUCTION

Spall fragments produced behind armor during impact must be characterized in detail so that damage potentials of shaped charges and other penetrating devices can be assessed adequately. The characterization usually consists of mass distributions, directions of travel and individual fragment velocity or speed. Such descriptions have traditionally been obtained by collecting fragments after each field test through the use of a relatively soft recovery medium such as wall board. At present, another technique, time sequenced flash x-rays of spall just after formation is being developed to complement or replace the recovery (collection) method, but until improved further, the recovery technique is apt to remain in use. The recovery method is not without inherent limitations, particularly with respect to the ability to accurately determine the initial spall fragment velocity before impact with the recovery material. Thus, it is necessary to examine the technique from time to time for possible improvement.

The velocity determination is obtained through use of an empirical equation calibrated for the recovery material utilized. Generally such equations provide a relationship between the striking velocity and penetration depth for given fragments with known masses. The presented areas of the fragments are a variable of the system and in practice are either measured or assumed. Simulated fragments such as spheres, cubes or short cylinders are often used and in these cases the data obtained is rather uniform, but does include some scatter due to uncertainty in fragment orientation and variations in recovery material properties. The application of these equations to irregular spall fragments gives rise to considerably more uncertainty since the individual presented areas differ significantly. Further, presented areas associated with the extreme orientations create an even wider dispersion which is not easily taken into account.

Zook¹ includes a historical summary of such calibration equations. The most widely used calibration expressions are perhaps those determined empirically by Project Thor²,

-
1. Zook, John. "An analytical model of Kinetic Energy Projectile/Fragment Penetration." BRLMR 2797, October 1977
 2. Ballistic Analysis Laboratory, Johns Hopkins University. Project Thor Technical Report No. 50: "The Calibration of a Collection Medium for the Determination of Particle Velocity." July 1962.

Whiteford and Regan³, and Collins⁴. The mathematical expression, $V = KM^a P^b A^c$, appears in their work together with an evaluation of the constants, K, a, b, and c fitted to various sets of data which reflect a number of wall board materials and fragment characteristics.

In the expression, V is the striking velocity and M, P and A are respectively the mass, penetration depth, and the average cross sectional area of the fragment type utilized. The inclusion of the variable A would presumably adjust the equation adequately for various fragment shapes (various average presented areas). However, an examination of various sets of constants show that they differ significantly as does the predicted velocity for a given set of fragment/penetration conditions.

II. THE MODEL

This study begins with the following hypothesis; The resistance force acting on a projectile during penetration of a thick impact medium (thick enough to bring the projectile to rest) is not constant. Near the beginning of penetration, where the velocity is high, the force is high and rapidly changing, similiar to a hydrodynamic drag force

$$f_1 = -k_1 v^2$$

At modest velocities, the force is derived from viscous effects:

$$f_2 = -k_2 v$$

Near the end of penetration, where the velocity is low, the force is primarily frictional, and essentially constant:

$$f_3 = -k_3$$

Apparently the exponent of v varies over the course of the penetration. In terms of the dependent variable, one can say the exponent of v varies over the range of v. Therefore, the exponent of v is itself a function of v, varying from nearly 2 at the beginning of penetration to nearly 0 at the end.

3. Whiteford, C. W. and Regan, J. M., "The Determination of the Striking Velocity of Steel Fragments by their Mass and Penetration into Witness Material", BRLMR-1333, April 1961.
4. Collins, John A. "Fiberboard Calibration for Determination of Fragment Velocities", Eglin Air Force Base Technical Report AFATL-TR-73-193, September 1973.

Algebraically, then, the assumed basis of this model is:

$$f = -kv g(v)$$

In this force law g is some function of v for which

$$0 < g < 2 \quad \text{for} \quad 0 \leq v \leq v_0$$

where v_0 is the striking velocity. This is all that is known about the function g . Since most functions can be represented by a polynomial (e.g. Taylor series), this is a logical choice for g . Specifically, a single term "polynomial" is chosen for simplicity. Thus the assumed velocity dependence is:

$$g(v) = \alpha v^a$$

In the force law $k = k(v)$ to the extent of reconciling dimensions (i.e. numerically constant, dimensionally variable). Following conventional theory, the constant depends on the density of the medium being penetrated (ρ) and the presented area of the projectile (A). Finally,

$$f = -c\rho A v^{\alpha a}$$

where c is a calibration constant for the impact medium (i.e. determined by calibration experiments), ρ is the density of the impact medium, A is the presented area of the projectile, and α and a are as yet unknown constants. They must, however, be positive to fit the model presented. Note that at this point conventional dimensional analysis will yield the familiar hydrodynamic drag force, $C_D \rho A v^2$.

Since the exponent must be dimensionless, let

$$\alpha = \gamma / v_0^a$$

where γ is a dimensionless constant (as yet unknown). Thus:

$$f = -\rho c A v \left(\frac{v}{v_0} \right)^{\alpha a} \quad (1)$$

Inspection of Equation 1 reveals that $\alpha = 2$ and $a \neq 0$ is required if the exponent is to vary from 0 to 2. The polynomial form of the approximation of the exponent is not valid at $v = 0$, since it leads to a non-zero force there. In lieu of choosing a two term polynomial for the exponent, (e.g. $\alpha v^a + \beta$) the range of v will be limited to $v/v_0 > 0$. This will cause no inconvenience in the analysis of actual experimental data, nor will it result in any appreciable error.

From Newton's second law, if the recovery medium causes no erosion of the projectile:

$$M \frac{dv}{dt} = -\rho c A v^2 (v/v_0)^a \quad (2)$$

where M is the mass of the projectile. Now the derivative may be rewritten as follows. Since $v = v(x,t)$,

$$dv = \frac{\partial v}{\partial x} dx + \frac{\partial v}{\partial t} dt$$

$$\frac{dv}{dt} = \frac{\partial v}{\partial x} \frac{dx}{dt} + \frac{\partial v}{\partial t}$$

but

$$\frac{\partial v}{\partial t} = 0$$

$$\frac{dv}{dt} = \frac{dv}{dx} \frac{dx}{dt}$$

where dx/dt is simply v . Substituting into Equation 2 will yield the velocity as a function of penetration depth, x .

$$Mv \frac{dv}{dx} = -\rho c A v^2 (v/v_0)^a$$

Separating:

$$v^{1-2(v/v_0)^a} dv = -\frac{\rho c A}{M} dx \quad (3)$$

Both sides are integrated over the course of the penetration:

$$-\frac{\rho c A}{M} \int_0^P dx = \int_{v_0}^1 v^{1-2(v/v_0)^a} dv$$

where P is the penetration of the projectile at $v \rightarrow 0$, approximately equal to the total penetration.

$$\frac{\rho c A}{M} P = \int_1^{v_0} v^{1-2(v/v_0)^a} dv \quad (4)$$

III. APPLICATION OF THE MODEL: METHOD I

Equation 4 contains two calibration constants, a and c . To evaluate these two unknown empirical constants, recall that c is a constant associated with the impact medium, and is not a

function of projectile area, mass or velocity (assumedly). Thus the second "equation" needed to evaluate the two unknowns a and c is c = constant, and the value of a is sought which best satisfies this condition.

Collins' impact medium calibration using 57 mg steel spheres (Table A-1) is used as an example. Equation 4 is solved for c.

$$c = \frac{M}{\rho AP} I(v_0) \quad (5)$$

where

$$I(v_0) = \int_1^{v_0} v^{1-2(v/v_0)^2} dv \quad (6)$$

represents the integral on the right in equation 4. In Collins' test, the impact medium was Celotex, with a density of

$$\rho = 272 \text{ kg/m}^3 \quad (7)$$

For 57 mg spheres,

$$M = 5.7 \times 10^{-5} \text{ kg} \quad (8)$$

The presented area at impact is constant for all orientations, and is found from the sphere's mass:

$$A = 4.54 \times 10^{-6} \text{ m}^2 \quad (9)$$

$$R = 1.20 \times 10^{-3} \text{ m} \quad (10)$$

Substituting equations 7, 8, and 9 into Equation 5:

$$c = .04616 \frac{I(v_0)}{P} \quad (11)$$

Collins' calibration data (Table A-1) gives v_0 and P for numerous shots of the steel spheres into the Celotex impact medium. Tests yielding penetrations of less than .051m showed erratic results, and so were disregarded in this study. The following method was used to evaluate a and c: a is a parameter, and is assigned various values. For a given data

point (P, v_0) , I is found by numerical integration of Equation 6. The trapezoidal rule with 1000 uniform intervals was used for accuracy consistent with the accuracy of the data. The value for I and the corresponding value for P (for the given data point) is then substituted into equation 11 to determine c .

This procedure is repeated for each data point (P, v_0) and the mean (\bar{c}) and standard deviation (σ) of the resulting values of c are computed. A new value for the parameter a is then assumed, and the whole process is repeated. Since c should be constant, σ should be zero. Of course, this is not reasonable in an experiment. Instead, a minimum is sought. σ is normalized by the mean (\bar{c}) and σ/\bar{c} is plotted versus the parameter a . This is done in Figure 1. A clear minimum exists. Thus we conclude that the proper value of the parameter a is

$$a = 0.20 \quad (12)$$

For this choice of a , Collins' 57mg sphere calibration data leads to an average value for c of

$$c = 50.3 \quad (13)$$

The computations are summarized in Table 1, and were obtained from Equation 5 with numerical integration of Equation 6. We are now ready to use Equation 4 to predict the velocity of fragments impacting the Celotex impact medium. Collins' data for small fragments (approximately the same mass as the calibration spheres), presented in Table A-2, will be studied.

First Equation 5 is rewritten

$$I(v_0) = \frac{\rho c A}{M} P \quad (14)$$

Now $I(v_0)$ is defined by equations 6 and 12. $I(v_0)$ can be numerically integrated and plotted as a function of v_0 . This is done in Table 2 and Figure 2; the relationship turns out to be nearly linear. This simplifies the prediction of fragment velocities, since a graphical solution is not required. For velocities greater than 100m/s, the equation of the curve in Figure 2 is:

$$I(v_0) = \frac{v_0}{10} + 8 \quad (15)$$

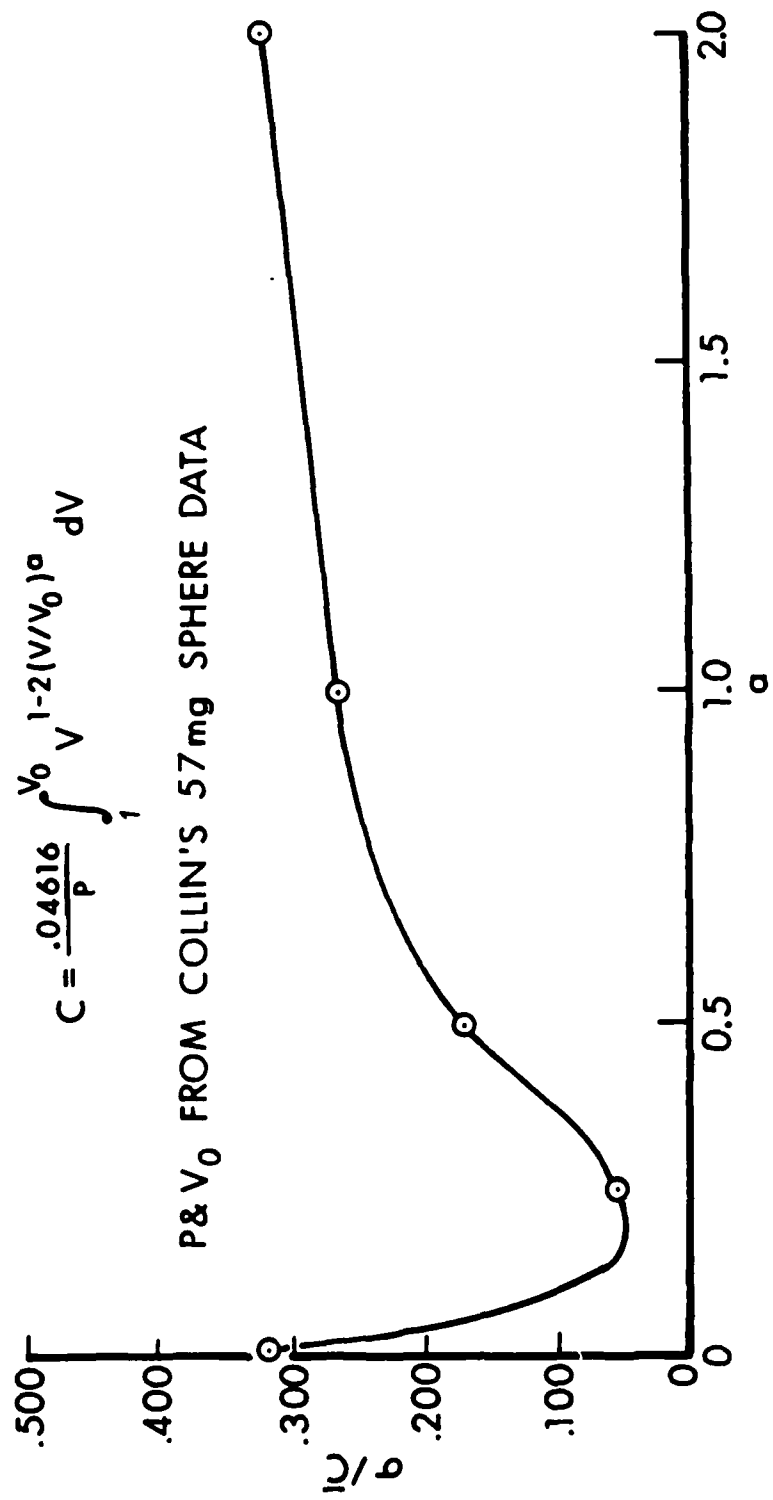


FIGURE 1. Parametric Variation of Calibration Data.

Table 1. Computation of Impact Medium Calibration Constant c.

v_o	P	c	$I(v_o)$
1606.	.155	50.10	168.23
1602.	.155	49.98	167.83
1600.	.155	49.92	167.64
1588.	.148	51.92	166.46
1567.	.151	50.26	164.40
1535.	.138	53.94	161.27
1529.	.151	49.12	160.68
1479.	.135	53.27	155.79
1375.	.133	50.53	145.60
1369.	.138	48.51	145.02
1362.	.135	49.35	144.33
1354.	.135	49.08	143.55
1351.	.141	46.90	143.25
1340.	.135	48.61	142.18
1331.	.135	48.31	141.30
1023.	.106	48.39	111.13
1015.	.106	48.05	110.35
1007.	.099	51.09	109.56
995.	.104	48.11	108.39
993.	.101	49.45	108.19
988.	.101	49.22	107.70
978.	.106	46.47	106.72
969.	.098	49.85	105.83
962.	.098	49.53	105.15
962.	.098	49.53	105.15
787.	.077	52.71	87.93
753.	.077	50.70	84.58
693.	.077	47.14	78.64
691.	.071	51.00	78.44
672.	.064	55.22	76.56
663.	.071	49.19	75.67
652.	.071	48.48	74.58
652.	.064	53.79	74.58
621.	.064	51.56	71.49
617.	.064	51.28	71.10
615.	.057	57.41	70.90
612.	.064	50.92	70.60
565.	.057	53.37	65.91

Table 2. Numerical integration of the integral.

v_o	INTEGRAL
100.	16.90
200.	28.27
300.	38.93
400.	49.26
500.	59.39
600.	69.40
700.	79.34
800.	89.22
900.	99.06
1000.	106.88
1100.	118.68
1200.	128.47
1300.	138.36
1400.	148.05
1500.	157.84
1600.	167.64
1700.	177.44
1800.	187.26
1900.	197.08
2000.	206.91

Thus equation 4 can be rewritten

$$\frac{\rho c A}{l} P = \frac{v_o}{10} + 8$$

Despite the complexity of the original model, the depth of penetration of the projectile is simply directly proportional to the striking velocity (this may not be the case for other sets of data). Rearranging,

$$v_o = \frac{10 \rho c A}{M} P - 80 \tag{16}$$

Substituting $\rho = 272 \text{ kg/m}^3$ and $c = 50.3$

$$v_o = 1.37 \times 10^5 \frac{A}{M} P - 80 \tag{17}$$

This can be written in the general form

$$v_o = \beta \left(\frac{AP}{M} \right) + b \tag{18}$$

where β is the slope and b the ordinate intercept of the line.

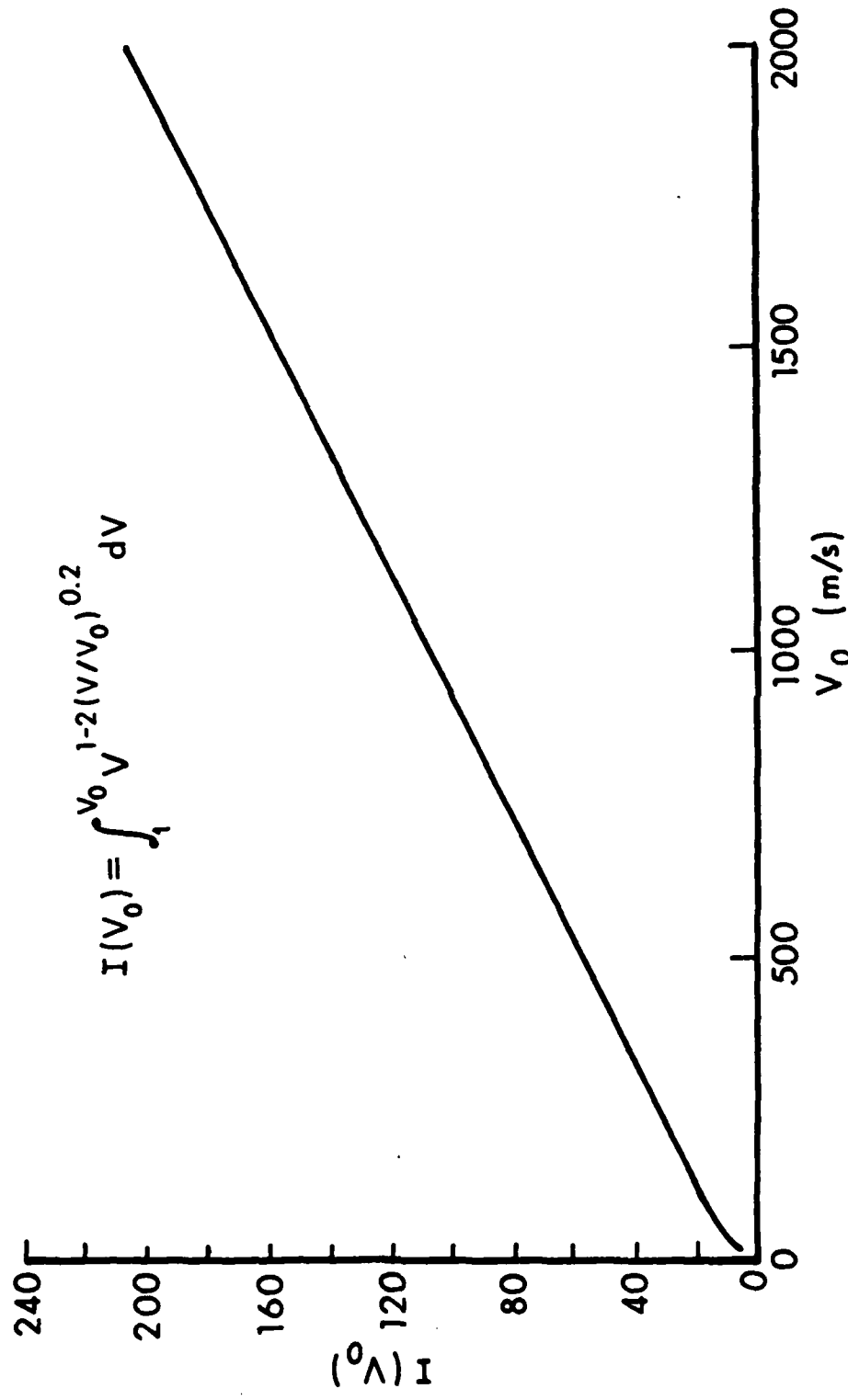


FIGURE 2. Approximation of the Integral.

Collins' data for small fragments (see Table A-2) is plotted in Figure 3. Fragments for which v_0 was less than 100m/s were disregarded (total of three). A linear regression of this data was performed, with the following results:

$$\begin{aligned} \text{slope } (\beta) &= 1.14 \times 10^5 \text{ kg/m}^2 \text{ s} \\ \text{ordinate intercept } (b) &= 143 \text{ m/s} \end{aligned}$$

This line is plotted in Figure 3 as the solid (actual) line. Also plotted is the dashed (predicted) line, which is based on

$$\begin{aligned} \text{slope } (\beta) &= 1.37 \times 10^5 \text{ kg/m}^2 \text{ s} \\ \text{ordinate intercept } (b) &= -80 \text{ m/s} \end{aligned}$$

from Equation 17 above. A close look at Figure 3 reveals that for impact velocities between 1000 and 1500 m/s, the described method predicts within $\pm 5\%$ of the true value and within $\pm 10\%$ between 800 and 2600 m/s. The error at 200 m/s is about $\overline{100\%}$. The method is more accurate at high impact velocities by virtue of the exponent of v . Also, one would expect more consistent penetration data at high velocities. Also, recall that Equation 17 is not valid at striking velocities less than 100 m/s (e.g. penetration at or near zero must be excluded from consideration).

IV. SIMPLIFYING THE MODEL

Consider the velocity of the projectile as it penetrates the recovery medium. Equation 3 is integrated from 0 to x and from v_0 to $v(x)$. $a = 0.2$ from Collins' data was used for definiteness, although $a = 1$ was also tried with similar results.

$$-\rho c \frac{A}{M} \int_0^x dx = \int_{v_0}^{v(x)} v^{1-2(v/v_0)^{0.2}} dv \quad (19)$$

To simplify notation, the integrand will be referred to as $f(v)$. Solving for x ,

$$x = -\frac{1}{\rho c} \frac{M}{A} \int_{v_0}^v f(v) dv \quad (20)$$

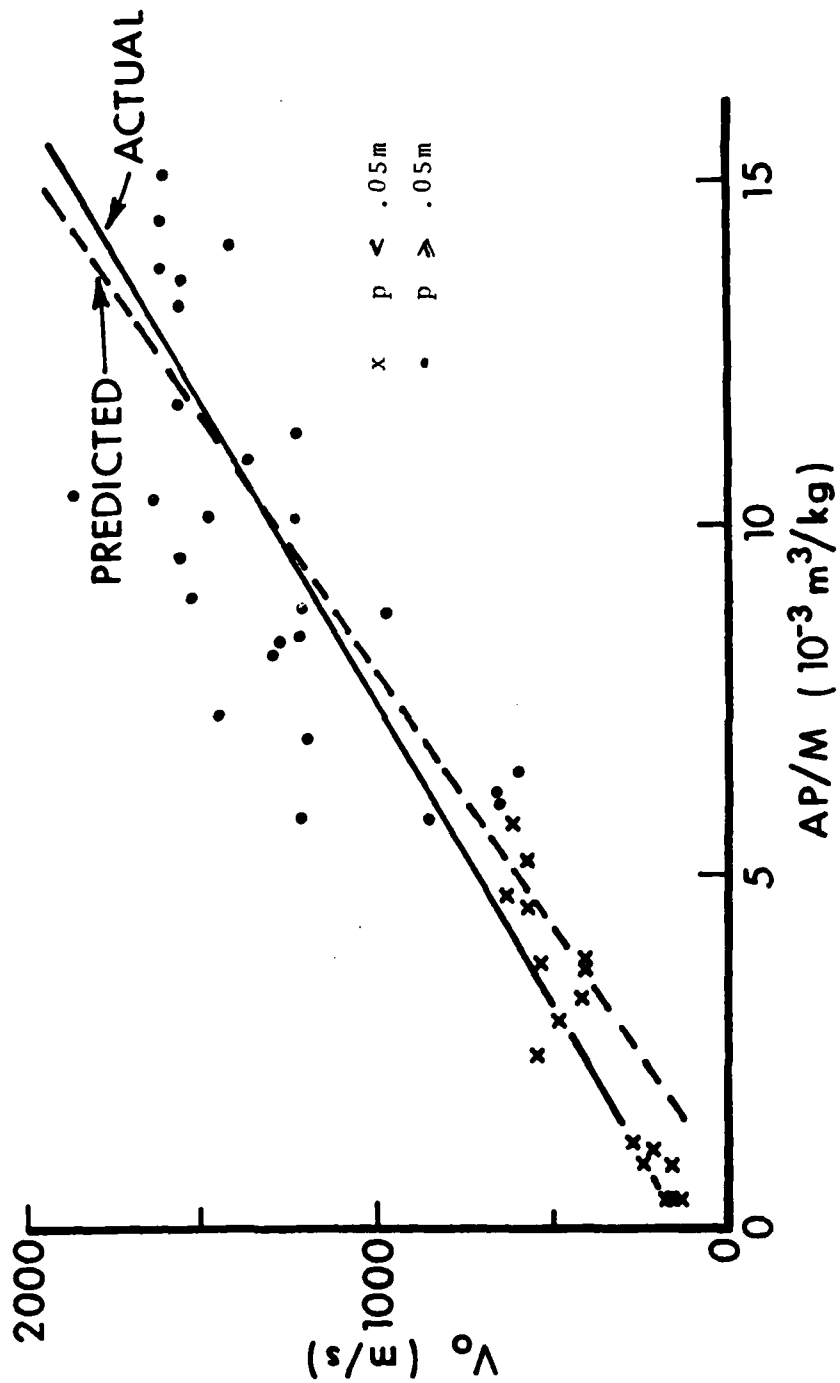


FIGURE 3. Results of Method I.

Reducing the equation to the customary form $v = v(x)$ is not possible, so the following discussion will be somewhat awkward. The integrand $f(v)$ is plotted in Figure 4. The independent variable is of necessity v , the instantaneous projectile velocity. For any striking velocity v_0 and instantaneous projectile velocity v , the area under the appropriate v_0 curve between v_0 and v (as a fraction of the total area under the v_0 curve) is proportional to the depth in the impact medium at which the velocity v is reached (as a fraction of the total depth penetrated).

Figure 4 thus gives important insight into the model. The projectile slows down extremely rapidly in the beginning of its penetration into the medium; approximately one-half of its velocity is lost in the first one-tenth of penetration. Thus the hydrodynamic regime, where the resistance force is proportional to v^2 , is over very quickly, with little contribution to the total penetration. In fact, the great majority of the penetration occurs in a narrow band of velocity exponent, say from $1/4$ to $3/4$. Thus assuming a constant value for the exponent of velocity in the resistance relationship is reasonable. This assumption should lead to acceptable accuracy over a sizable range of striking velocity provided the value of the exponent is chosen properly. How is this done?

To begin, the resistance force (Equation 1) with $a = 0$ will result in a constant for the velocity exponent:

$$f = -\rho c A v^\gamma \quad (21)$$

where γ is a constant to be determined. This force is zero at $v = 0$, so the range of applicability of v is $0 \leq v \leq v_0$. Equation 4 now becomes:

$$\rho c \frac{A}{M} P = \int_0^{v_0} v^{1-\gamma} dv \quad (22)$$

To avoid the singularity at $\gamma = 2$, Let

$$\gamma = 2 - \frac{1}{\beta} \quad 0 < \beta < \infty \quad (23)$$

β turns out to be a more useful parameter than γ .

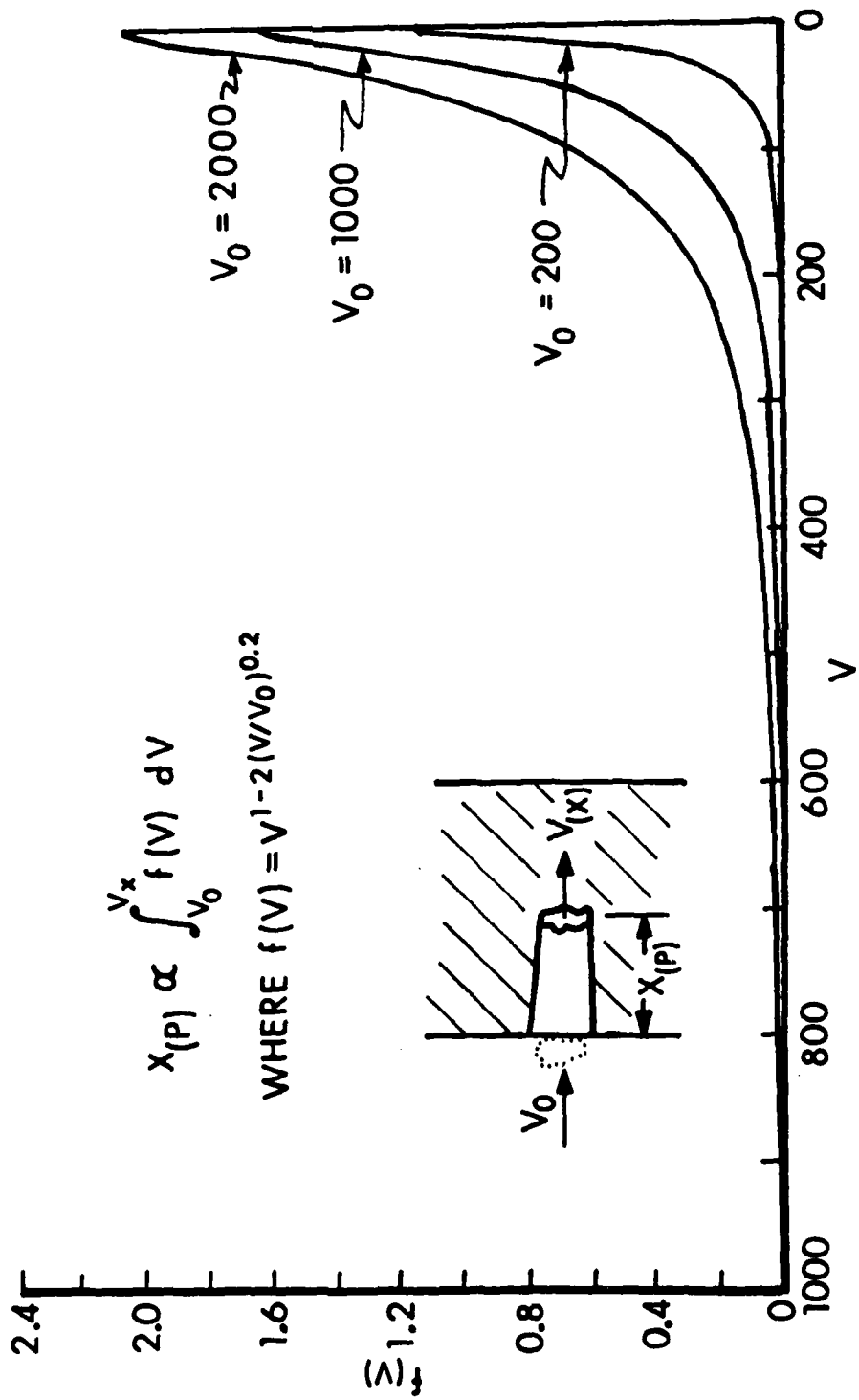


FIGURE 4. Fragment Penetration as a function of Instantaneous Fragment Velocity.

Substituting:

$$\rho_c \frac{A}{M} P = \int_0^{v_0} v^{1/\beta - 1} dv$$

Integrating:

$$\rho_c \frac{A}{M} P = \beta v_0^{1/\beta} \quad (24)$$

This can be rewritten

$$v_0 = \left(\frac{\rho_c}{\beta} \right)^\beta M^{-\beta} A^\beta P^\beta \quad (25)$$

which has the mathematical form extensively used for velocity calibration of recovery media as indicated previously. Note that $\beta = 1/2$ is the solution for a constant resistive force, $\beta = 1$ represents a force proportional to the first power of the velocity, and $\beta \gg 1$ corresponds to the hydrodynamic drag force.

V. COMPARISON TO EXISTING CALIBRATION EXPRESSIONS

In this section Equation 25 is compared to calibration expressions (having the same form) as utilized by Project Thor(ref 2), Whiteford and Regan(ref 3), Collins(ref 4), and others. One form frequently encountered is

$$v_0 = K_1 M^a P^b A^c \quad (26)$$

In cases where fragment area and mass can be assumed to be related by $A = KM^{2/3}$ (see discussion of Method IV below), another common expression results in

$$v_0 = K_2 M^g P^b \quad (27)$$

The exponents a, b, c, g, and the coefficients K_1 and K_2 are given in calibration determinations as elements of regression analyses and in general are not constrained to maintain any given relationship between themselves. However, the current assumed model (Equation 25) indicates that a definite relationship exists between exponents, namely

$$-a = b = c \quad (28)$$

$$-g = 1/3 b \quad (29)$$

These relations were tested by sets of empirically determined exponents originally determined for the equations 26 and 27. The work of several investigators was used, and is summarized in Table 3. In all cases the fragments considered were steel. Further details of the tests may be found in the cited references.

The comparisons provided by the table indicate that the empirical ratios are close to those predicted by the model. The ratios appear to be very close for data representing spherical, cubicle, or short cylindrical ($l/d = 1$) fragments. However, there is a greater difference for data obtained in tests where fragments had more extreme shapes (bomb, weapon, and bomblet fragments). The departures are caused by unavoidably inaccurate measurements of the average presented area of fragments, rotation of the fragment during penetration (i.e. variation of presented area) and other problems in a real fragmentation experiment. Affecting calibration shots as well as fragmentation experiments are such factors as instrumentation accuracy and collection medium homogeneity. The fact that Equation 25 (and hence Equations 28 and 29) results from an approximation to the originally proposed model may also contribute to the differences, depending on the validity of the original model.

The favorable comparisons obtained with the more ideal shapes lend credence to the approach taken here. Hence, the theory provides the basis for further examination of the factors involved in the calibration process.

Historically, the exponents and lead constants are applied collectively in any given expression. Thus although they may vary from the theoretical values because of the quality of fit, amount and quality of data, etc., their collective application provides reasonable predictions of velocity over the range of applicability of the calibration measurements. However, if the exponents are related as prescribed above, one would expect a simplification of the calibration process and a better fit over the rest of the data.

VI. APPLICATIONS OF THE SIMPLIFIED MODEL

A. Calibration

Equation 25 is the starting point in reducing experimental data. It is repeated here for reference.

$$v_o = \left(\frac{\rho c}{B} \right)^\beta M^{-\beta} A^\beta P^\beta \quad (25)$$

Table 3 - Evaluation of Equations 28 and 29 by Empirically determined constants.

Eq 28 : $-a = b = c$
 Eq 29 : $-g = 1/3 b$

Investigator	Recovery Material	Ref.	Frag. Type	a	g	b	c	-a/b	c/b	-c/a	-g/b	current model
Project Thor	MAFTEX	2	cy1 & sph	-.681		.736	.638	.925	.867	.937		1
Project Thor	MAFTEX	2	cy1 & sph		-.255	.736					.346	1/3
MALICK	NU-WOOD	5	cy1	-.939		.809	.908	1.161	1.122	.967		1
MALICK	NU-WOOD	5	cy1		-.336	.809					.415	1/3
Whitford and Regan	PLASTERGON	3	cube		-1/3	1					1/3	1/3
Collins	NU-WOOD	4	sph		-.302	.719					.420	1/3
Collins	NU-WOOD	4	Sph & bomb	-.625		.698	.523	.895	.750	.837		1
Collins	NU-WOOD	4	Wpns	-.497		.727	.547	.684	.752	1.10		1
Killen	NU-WOOD		Plate	-.532		.896	.447	.594	.499	.840		1

The constants c and β are determined by calibrating the impact medium by firing known fragments at known (measured) velocity into the medium. Spheres are used here because of ease of launching and their known presented area (A is independent of the sphere's orientation at impact).

To determine c and β from the calibration data, rewrite Equation 25:

$$v_o = \left(\frac{\rho c A P}{\beta M} \right)^\beta \quad (30)$$

Now substitute $A_{\text{sphere}} = \pi R^2$ and $M_{\text{sphere}} = \rho_s \left(\frac{4}{3} \pi R^3 \right)$

$$v_o = P^\beta \left[\frac{3}{4} \frac{c}{\beta} \frac{\rho}{\rho_s} \frac{1}{R} \right]^\beta \quad (31)$$

$$\ln v_o = \beta \ln P + b_1 \quad (32)$$

where

$$b_1 = \beta \ln \left(\frac{3}{4} \frac{c}{\beta} \frac{\rho}{\rho_s} \frac{1}{R} \right) \quad (33)$$

v_o Striking Velocity of fragment, m/s

ρ Mass density of impact medium (Celotex) = 272 kg/m³

ρ_s Mass density of sphere (steel) = 7833 kg/m³ (489 lb/ft³)

c Constant dependent on impact medium, (m/s)^{1/\beta}

β Constant dependent on impact medium (dimensionless)

P Depth of penetration of fragment into impact medium, m

M Mass of fragment, kg

R Radius of the steel calibration sphere, m

β and b_1 in Equation 32 are determined from a linear regression analysis of the calibration data. c is then determined from:

$$c = \frac{4}{3} \frac{\rho_s}{\rho} RB \exp (b_1/\beta) \quad (34)$$

Table A-1 shows velocity and penetration of 57 mg steel spheres into a particular impact medium. The data is plotted in Figure 5. Regression analysis indicates:

$$\begin{aligned} \beta &= 0.672 \\ b_1 &= 8.448 \end{aligned}$$

and in Equation 34:

$$c = \frac{4}{3} \frac{7833}{272} (1.20 \times 10^{-3}) (.672) \exp \frac{8.448}{.672}$$

$$c = 8924$$

These values of β and c are assumed to hold for any shape fragment that impacts this medium.

Tables A-3 through A-5 show similar data for other size spheres (700mg to 1059mg). Regression analysis of these groups shows β and b_1 to vary slightly over this range of "fragment" mass, indicating that calibration spheres should be of approximately the same size as the fragment being studied. A given test therefore may require several sizes of calibration spheres. The model (Equation 25) does not predict any variation of β and b_1 (Equation 32) with mass. The existence of the variation is most likely due to variations in measurement of one or more of the variables ($M, A, P, \text{ or } v$). Table 4 shows the extent of the variations for Collins' data.

Although Equation 32 predicts a linear relationship between $\ln P$ and $\ln v_0$, when the actual data is plotted (Figures 5, 6, and 7), the data is seen to deviate from a straight line, especially at high velocities. Dividing the graphs into two more nearly linear regions does not make much difference in the "constancy" of β and b_1 over this range of mass (see Table 4).

Note also that grouping together all sphere data is apparently misleading, as it results in a lower slope (β) than any individual group, while not appreciably affecting the

Table 4. Variation with Fragment Mass of Calibration Constants β and b_1 .

MASS mg	N	Combined $0 < v < 8$		Separate $0 < v < 6$		Separate $6 < v < 8$	
		β	b_1	β	b_1	β	b_1
57	55	.672	8.45	.477	7.61	.994	9.20
700	69	.671	7.70	.474	7.02	.940	8.01
1025	101	.736	7.81	.333	6.48	1.070	8.17
ALL	225	.565	7.69	.263	6.37		

ordinate intercept, b_1 (high velocity behavior is similar). Physically, spheres of different mass impacting the medium at the same velocity will bring different amounts of energy to the collision, so one would expect them to penetrate differently; the more massive sphere penetrating more deeply. Presented area, being greater for the more massive sphere, will mitigate this effect. Thus, grouping together all sphere data is also physically incorrect.

B. Method II

The first simplification of the basic model assumes only a constant value for the exponent of v . The test must measure mass, presented area, and penetration into the calibrated medium for each fragment. Calibration of the impact medium (see above) is also required. This type of data is presented in Table A-2, which was selected from Collins, Appendix J ("Small Fragment Data"), for fragments of approximately the same mass as the calibration spheres (57 mg.) Collins measured the velocity of these fragments electronically, and this data is also presented.

To predict fragment velocity, begin with Equation 25. Rewriting:

$$v_0 = \left(\frac{AP}{M} \right)^{\beta} \left(\frac{\rho C}{\beta} \right)^{\beta} \quad (35)$$

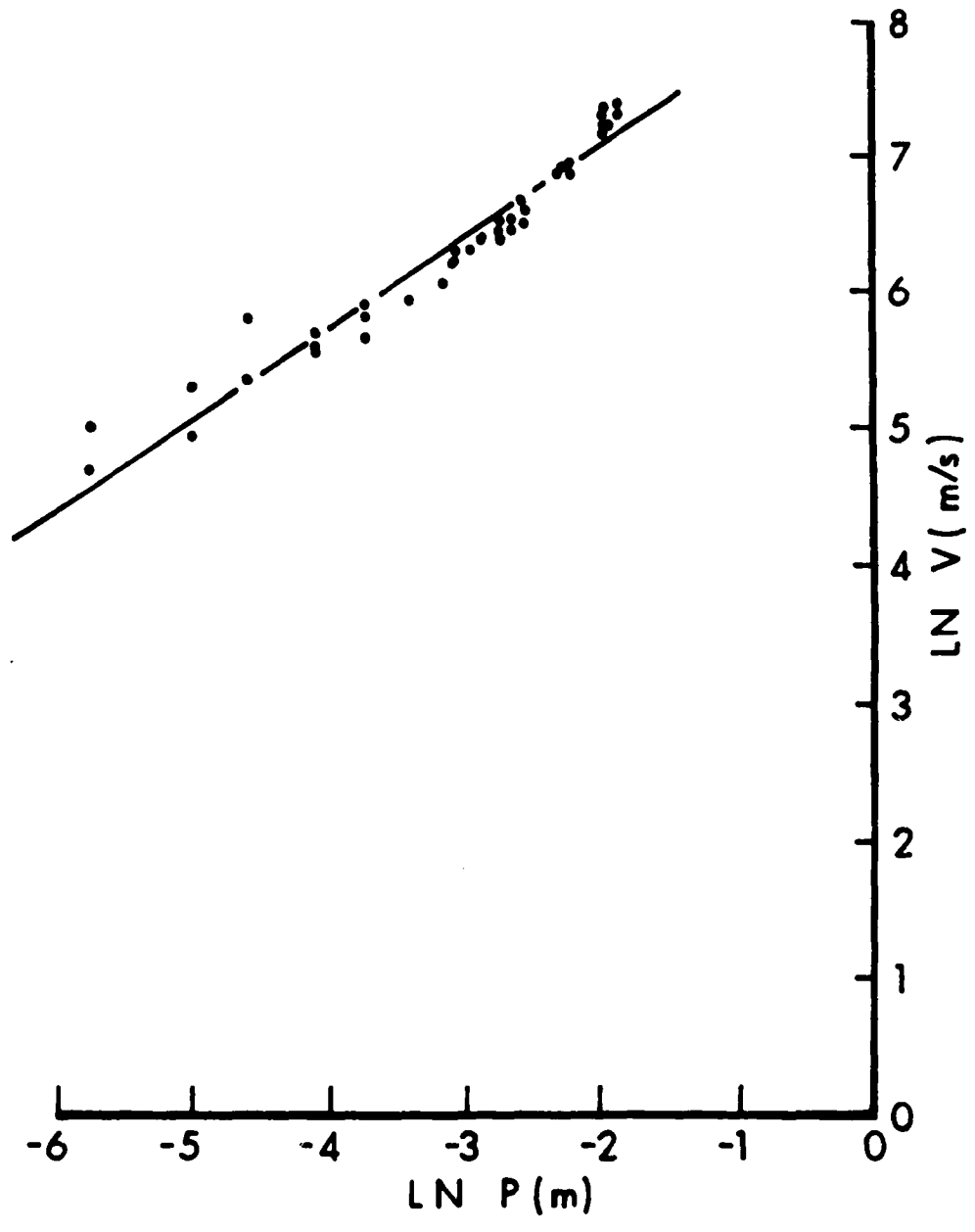


FIGURE 5. Sphere Calibration of Impact Medium Using 57mg Spheres.

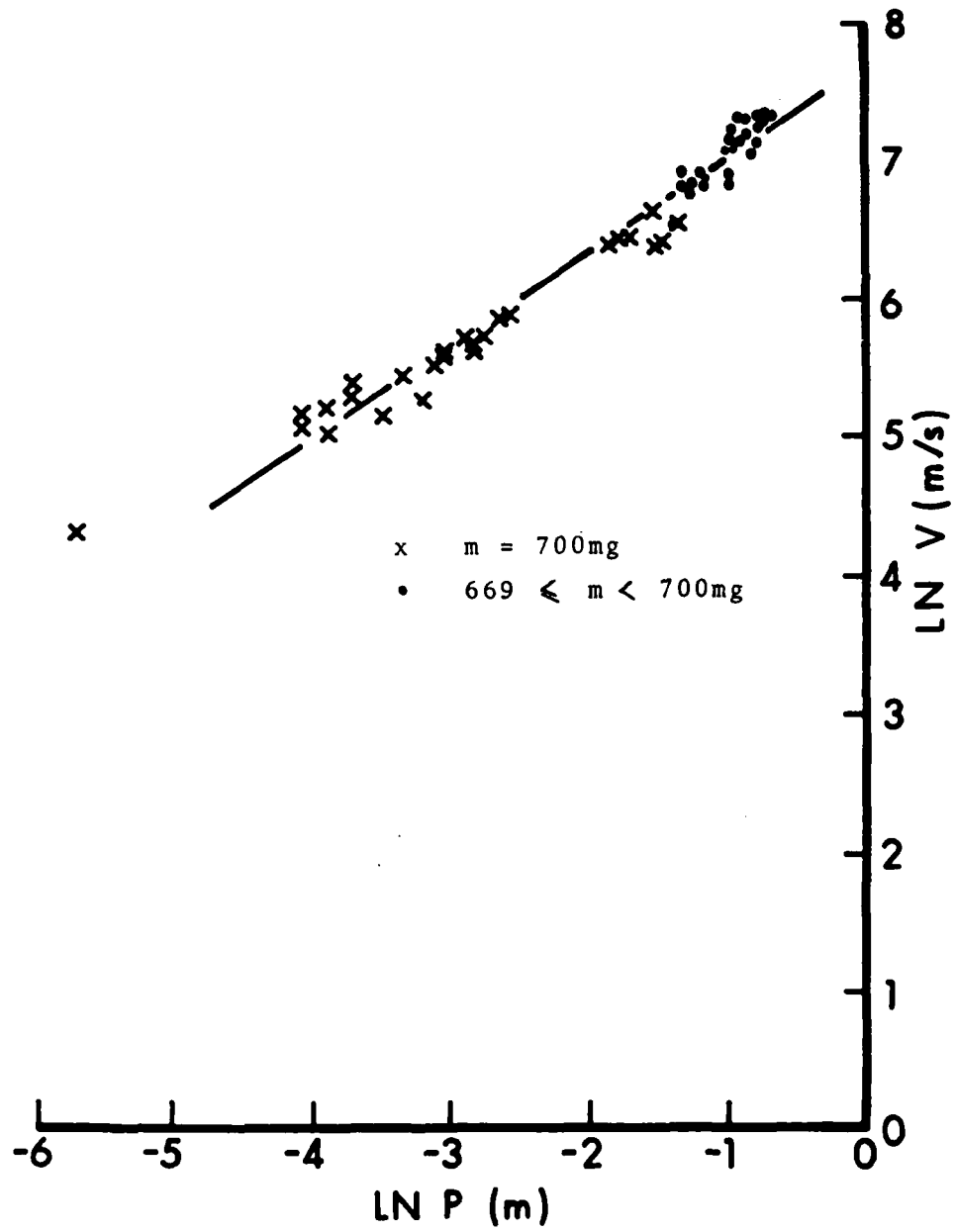


FIGURE 6. Sphere Calibration of Impact Medium Using 700mg Spheres.

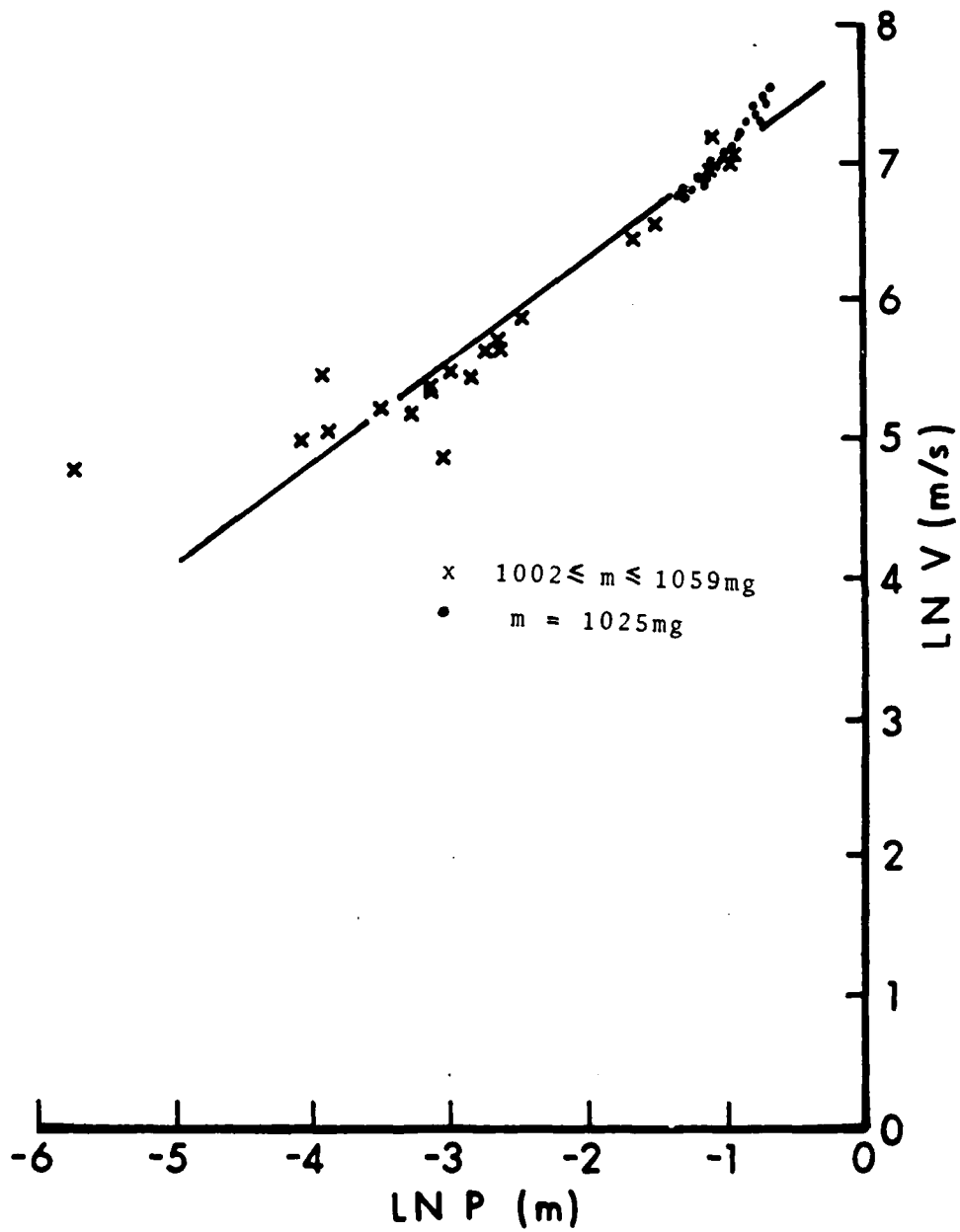


FIGURE 7. Sphere Calibration of Impact Medium Using 1025mg Spheres.

$$\ln v_o = \beta \ln \left(\frac{AP}{M} \right) + b \quad (36)$$

where

$$b = \beta \ln \left(\frac{\rho c}{\beta} \right) \quad (37)$$

β and c were found from the calibration of the impact medium, and A , P and M were measured, so v can be computed. From the sphere calibration data above,

$$\beta = 0.672$$

$$c = 8924$$

The calibrated value for b , from Equation 37 is:

$$b = 10.15$$

The true (from measured velocity data) values for β and b in Equation 36 are found by regression analysis of the velocity data in Table A-2:

$$\beta = 0.755$$

$$b = 10.60$$

The measured velocity data is plotted as the dots in Figure 8. The solid line is the result of a linear regression analysis of this data: the slope (β) is .755 and the ordinate intercept (b) is 10.60. Two other lines are plotted. The dashed line marked "Method II" is the regression of the predictions from method II, using $\beta = .672$ and $b = 10.15$. The dashed line marked "Collins" is the regression of velocity predictions based on the relationship $v = K M^a P^b A^c$. Here a , b , and c are Collins' values as given in Table 3 ("sph & bomb"). Also, $K = 7102$ was obtained from the 57 mg sphere calibration data (Table A-1). For this line, $\beta = .879$ and $b = 11.26$. The figure shows this method to be comparable in accuracy to Method II at the low and middle velocities, but at high velocity Method II is superior.

C. Method III

Several additional approximate methods exist. These methods significantly reduce the time and cost involved in conducting the test, but of course there is an additional sacrifice in accuracy.

The first of these methods avoids the need to measure mass and presented area for each fragment by introduction of a shape factor, defined by a statistical sampling of the fragment population.

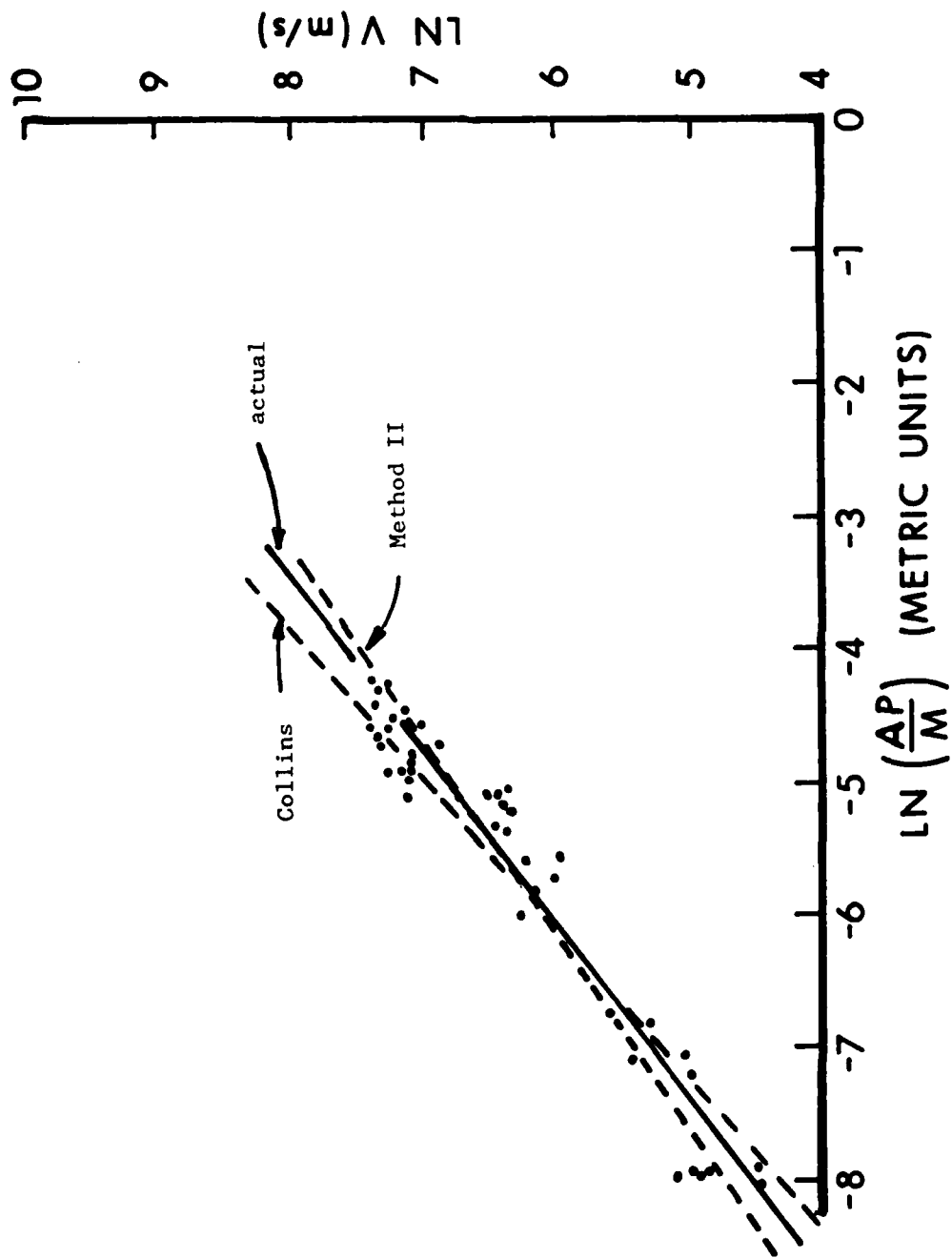


FIGURE 8. Results of Method II.

Define an average shape factor, k ; assumed valid for the entire fragment population:

$$A = kM^r \quad (38)$$

k may be found by measuring a statistically valid sample of the entire fragment population. If the sample is indeed valid this method can be very nearly as accurate as method II, as the example below will show. Note the subtle difference in the two methods: using A_i and M_i for each individual data point in method II was tantamount to using individual shape factors. Method III, of course, uses one average shape factor for all data points. From Equation 38:

$$\ln A = r \ln M + \ln k \quad (39)$$

Thus a linear regression analysis of fragment presented area and mass data will yield values for the constants r and k . The value of r thus determined is assumed valid for each individual fragment; it is a function of the entire population (class) of fragments.

Mass and area data for the small fragments under study are included in Table A-6. Using equation 39, a regression analysis of the data yields:

$$\begin{aligned} r &= 0.44 \\ k &= 5.56 \times 10^{-4} \quad (\ln k = -7.50) \end{aligned}$$

This was repeated for all fragment data (Table A-6 and Figure 9) resulting in $r = 0.42$ and $k = 4.69 \times 10^{-4}$. In this case the "statistically valid sample" is the entire population. In fact, the entire population breaks down as follows:

<u>Mass (mg)</u>	<u>n</u>	<u>r</u>	<u>k</u>
36 - 80	51	.44	5.56×10^{-4}
81 - 104	50	.30	1.44×10^{-4}
105 - 205	50	.40	3.79×10^{-4}
ALL	151	.42	4.69×10^{-4}

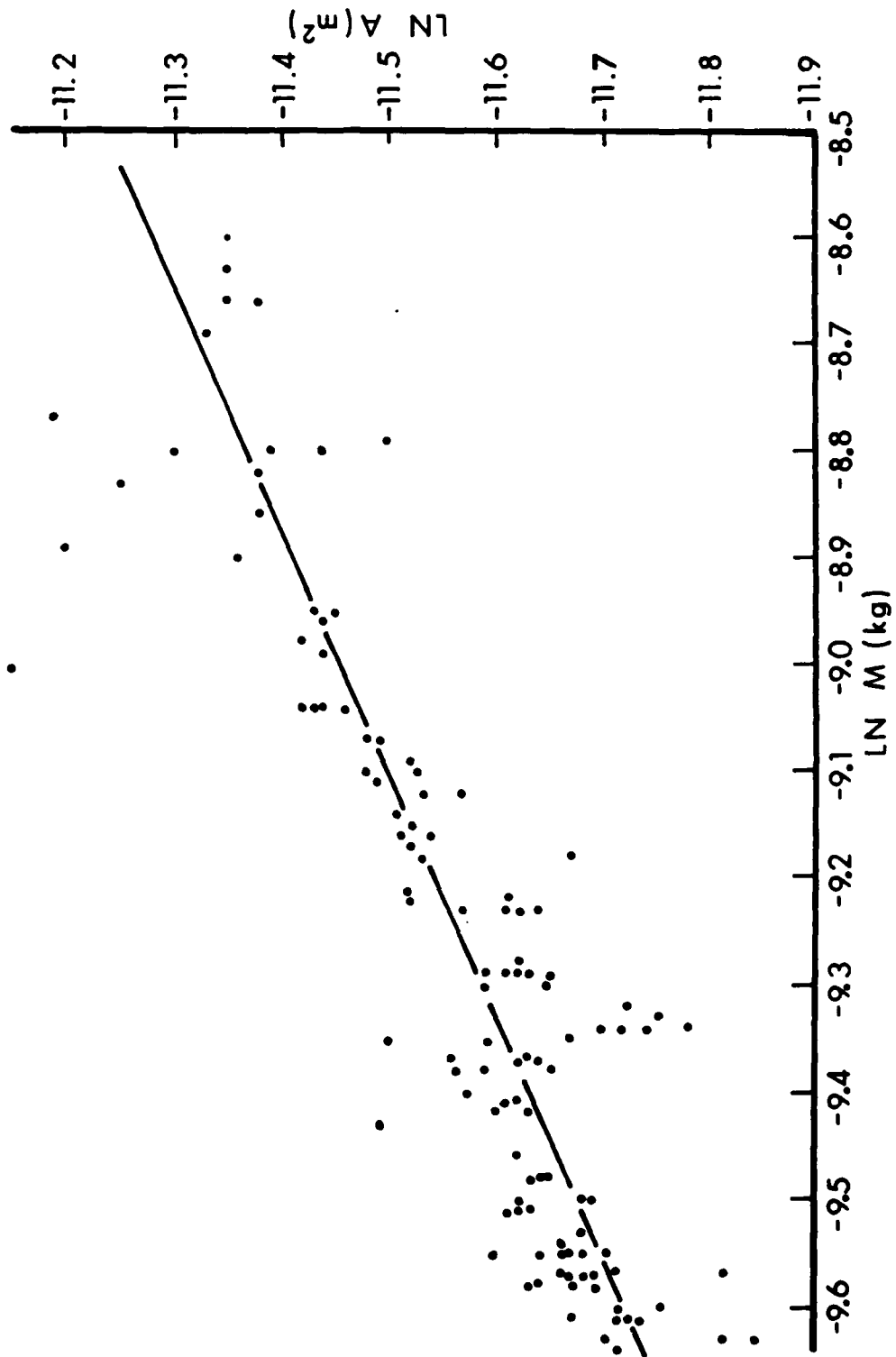


FIGURE 9. Relationship between Fragment Area and Fragment Mass for the Entire Fragment Population.

A similar analysis can be done to determine the degree of dependence of r and k on fragment area.

To utilize this method III, substitute Equation 38 into Equation 25:

$$v_o = \left(\frac{kP}{M^{1-r}} \right)^\beta \left(\frac{\rho c}{\beta} \right)^\beta \quad (40)$$

$$\ln v_o = \beta \ln \left(\frac{kP}{M^{1-r}} \right) + b \quad (41)$$

Where b is defined as Equation 37. From the sphere calibration data we get β and c , while r and k were found from the actual fragment data. So according to the method presented here, β and b are unchanged:

$$\beta = 0.672$$

$$b = 10.15$$

These may be compared to the results of a regression analysis of the data in Table A-2, based on Equation 41, with $r = .44$ and $k = 5.56 \times 10^{-4}$:

$$\beta = 0.770$$

$$b = 10.70$$

These results are plotted in Figure 10. The calculation was also carried out for the entire fragment population (Tables A-2 through A-5) with very little change: $\beta = .770$, $b = 10.69$ ($r = .42$, $k = 4.69 \times 10^{-4}$).

D. Method IV

This is the easiest method to apply, and potentially the most inaccurate. It assumes the relationship between fragment area and mass to be the same as that for spheres, and measures no fragment areas. To summarize the three simplified methods, each individual fragment's velocity computation is based on a relationship between that fragment's area and its mass determined from:

Method I and II. Direct measurement of each fragment's area and mass.

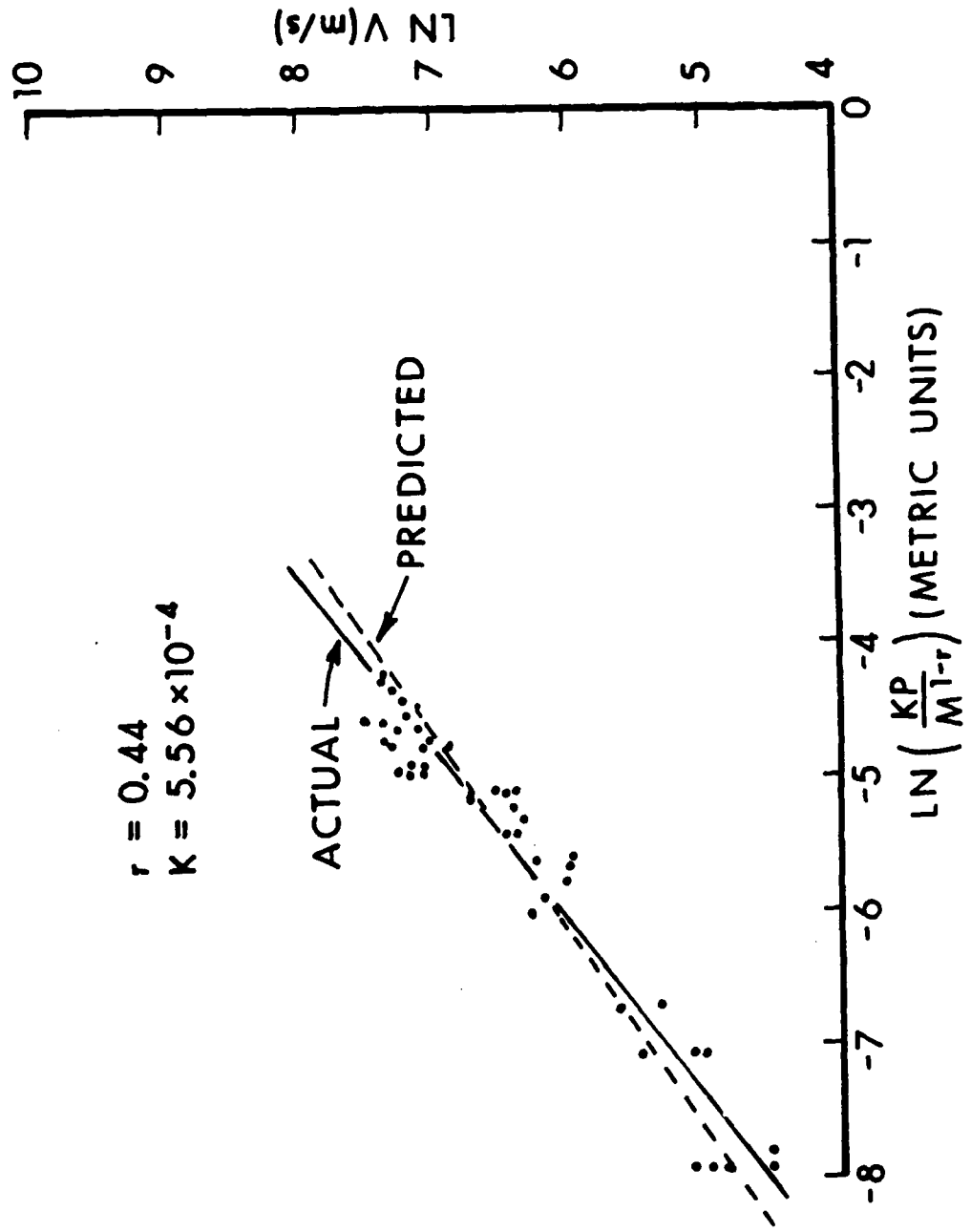


FIGURE 10. Results of Method III.

Method III. Measurement of fragment area for a sample of the entire population; but measurements of all fragment masses.

Method IV. Measurement of no fragment areas, but measurement of all fragment masses; relationship is that of spheres.

Equation 38 forms the basis of the approximation used to avoid the need of measuring each fragment's presented area.

$$A = kM^r$$

$$k = A/M^r$$

For spheres:

$$k = \frac{\pi R^2}{\rho_s^r \left(\frac{4}{3} \pi R^3\right)^r}$$

$$k = \rho_s^{-r} \left(\frac{3}{4}\right)^r (\pi)^{1-r} (R)^{2-3r}$$

The dependence on the radius will be removed if $r = 2/3$. In words, the proportionality between presented area and mass of a sphere will be independent of the size of the sphere. This is assumed to hold for all classes of homologous fragments. (See also reference 6 for a detailed discussion of shape factors).

For steel spheres:

$$k = (7833)^{-2/3} \left(\frac{3}{4}\right)^{2/3} (\pi)^{1/3} (R)^0$$

$$k = 30.65 \times 10^{-4} \quad (42)$$

Again substitute Equation 38 into Equation 25, set $r = 2/3$ and rearrange:

$$v_o = \left(\frac{kP}{M^{1/3}}\right)^\beta \left(\frac{\rho_c}{\beta}\right)^\beta \quad (43)$$

$$\ln v_o = \beta \ln \left(\frac{kP}{M^{1/3}}\right) + t \quad (44)$$

6. Dehn, James T. "Terminal Effectiveness, Vulnerability Methodology and Fragmentation Warhead Optimization. I. A Survey from an Historical Perspective." ARBRL-TR-02234, April 1980.

Here b is defined in Equation 37, the values for β and c were found with the sphere calibration data, and the value for k is that of Equation 42. Again, regression analysis using measured velocity data determines the experimental values for β and b . Equation 44 is the basis this time. The result is:

$$\beta = 0.763$$

$$b = 11.02$$

The data and regression fit are plotted in Figure 11 ("actual") along with the "predicted" fit ($\beta = .672$, $b = 10.15$). This is a remarkably good fit considering the arbitrary nature of the $r = 2/3$ assumption.

VII. CONCLUSIONS

Table 5 summarizes the various methods discussed, as applied to Collins' data (ref 4). It shows the values of the empirical constants ("calibration values"), which are computed from the calibration data, and it shows the equations in which they are used.

The slopes and intercepts of the "actual" curves in figures 3, 8, 10, and 11 are listed as the "true values" in Table 5. These values were found by substituting the measured data (fragment area, mass, striking velocity and penetration) into the relationships shown on the axes, and performing a linear regression of the results.

Two techniques are used to compare the accuracy of the methods. The first is based on visualization. In a graphical approach, the actual and predicted curves in one of the figures (3, 8, 10, or 11) are compared visually to assess the accuracy of the method. Similarly, an evaluation can be made using the calibration values and the true values found in Table 5. For example, Method II is more accurate than Methods III or IV because the empirical (calibration) values for β and b are closest to the true values (those that result from using measured velocities in the regression analysis instead of velocities computed with the equations listed in Table 5).

For comparison purposes, Table 5 includes information about the method used by Collins (and others). The "calibrated values" (empirical constants) used in this method are discussed on page 32 (Method II). The "true values" given for β and b are actually the result of a linear regression of the velocities computed by the equation given in the table. That is, they are not based on measured velocities, as are the other values given in these two columns. They are included here for comparison only; the main purpose for including this last line in Table 5 is for the accuracy comparison, which is discussed below.

The second technique for comparing the accuracy of the various methods is based on the linear regressions as well, but is more easily related to an experiment. This approach compares the range of true velocities for which the given model predicts velocities within 10% of the true velocity. It is based on the regression of each model's predictions as compared to that of the actual data. These values are presented in the last two columns of Table 5. One immediately sees that the easier to apply models are less

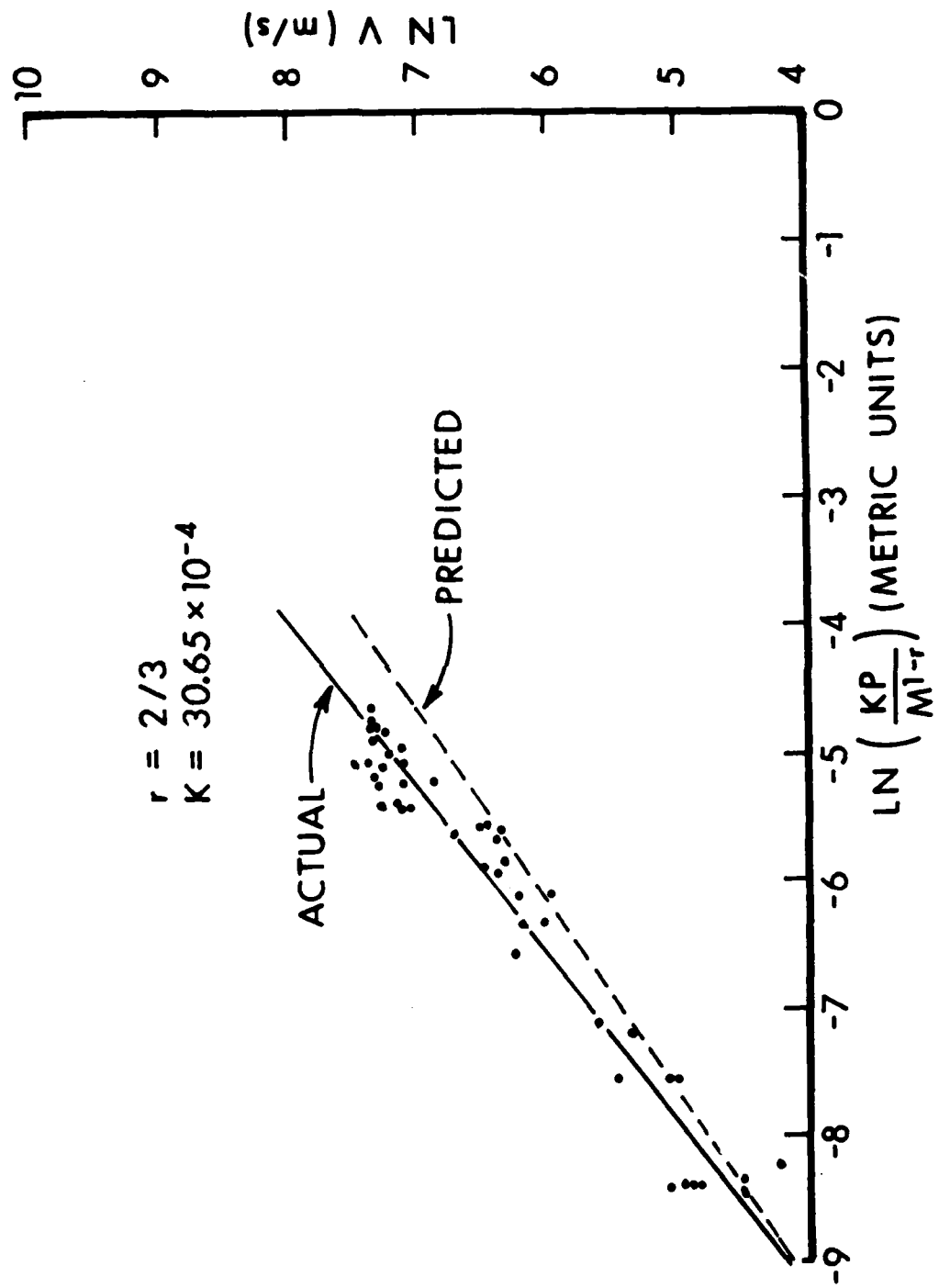


FIGURE 11. Results of Method IV.

Table 5. Summary of Methods

METHOD	CALIBRATION DATA		Relationship used	TEST DATA		
	calibration values	b		true (measured) values	$\pm 10\%$ Accuracy	v_0 Accuracy
	β			β	v_0 min	v_0 max
I	1.37×10^5	-80	$v_0 = \left(\frac{AP}{M}\right) \left(\frac{PC}{1/10}\right) + b$	1.14×10^5	840	2640
II	.672	10.15	$v_0 = \left(\frac{AP}{M}\right)^\beta \left(\frac{PC}{\beta}\right)^\beta$.755	280	1740
III	.672	10.15	$v_0 = \left(\frac{kP}{M^{1-T}}\right)^\beta \left(\frac{PC}{\beta}\right)^\beta$.770	300	1400
IV	.672	10.15	$v_0 = \left(\frac{kP}{M^{1/3}}\right)^\beta \left(\frac{PC}{\beta}\right)^\beta$.763	23	110
Collins			$v_0 = K M^a P^b A^c$.879	380	1290

accurate. The model studied in Method I results in the widest accurate range. As expected (see discussion of the technique above), it is the best for the higher velocities. This is due to the influence of the exponent of v in the resistance force relationship (Equation 1), and the fact that, at high velocities, the exponent is most accurately described in this method.

Method II sacrifices accuracy at high velocity by the simplifying assumption of a constant exponent of velocity in the resistance force expression (Equation 21). But it is a more accurate description at the low velocities, and it is an acceptable alternative in the current work.

As discussed above, Method III can be nearly as accurate as Method II if properly applied, and the accuracy figures support this contention.

Method IV has a poor accuracy range, and at best should only be used for the very low velocity fragments. However, it does provide some insight into the type of fragments that came off of this weapon at low velocities, in that the shape factor used was reasonable for these fragments.

The equation used by Collins in reference 4 (discussed in section IV above), has an accuracy of slightly less than Method III. Method II, with fewer approximations than Method III, shows a greater advantage in accuracy. The fact that Method II considers all exponents to be equal in magnitude lends credence to the discussion on that subject found in section IV.

The conclusions drawn above apply to the use of the equations with one particular set of data, and do not necessarily hold for other data sets.

Before closing, two additional approaches are discussed very briefly. First, the possibility of using a Taylor Series expansion of f in Equation 1 seems to have merit, but has a major problem: the derivative of f does not simplify the integral in equation 4, since (eq. 4.2.53, ref 7):

$$\frac{d}{dv} v^v = (1 + \ln v) v^v$$

Second, the following empirical formulation for a velocity dependent resistive force was suggested by J. Dehn as a possible alternative.

$$f = \frac{k (v/v_0)}{\ln[1+(v/v_0)]}$$

L'Hospital's rule shows that this force has a limiting value of k as $v \rightarrow 0$, and a limiting value of infinity as $v \rightarrow \infty$. These limits are the same as those for the Poncelet equation ($f = a + bv + cv^2 + \dots$). Substitution into Newton's law yields the following (the same as Equation 25, with $\beta = \frac{1}{2}$).

REFERENCES

1. John Zook, "An analytical Model of Kinetic Energy Projectile/Fragme . Penetration," Ballistic Research Laboratory MR 2797, October 1977.
2. Ballistic Analysis Laboratory, Johns Hopkins University. Project Thor Technical Report 50: "The Calibration of a Collection Medium for the Determination of Particle Velocity". July 1962.
3. Whiteford, C. W. and Regan, J. M. "The Determination of the Striking Velocity of Steel Fragments by their Mass and Penetration into Witness Material". Ballistic Research Laboratory MR 1333, April 1961.
4. Collins, John A. "Fiberboard Calibration for Determination of Fragment Velocities," Eglin Air Force Base Technical Report AFATL-TR-73-193, September 1973.
5. Malick, Donald. "The Calibration of Wallboard for the Determination of Particle Speed". Ballistic Analysis Laboratory, Johns Hopkins University, Technical Report 61, May 1966.
6. Dehn, James T. "Terminal Effectiveness, Vulnerability Methodology and Fragmentation Warhead Optimization. I. A Technical Survey from an Historical Perspective." Ballistic Research Laboratory TR-02234, April 1980.
7. Abramowitz, M., and Stegun, I. (editors), Handbook of Mathematical Functions with Formulas, Graphs, and Mathematical Tables, National Bureau of Standards, Applied Mathematics Series 55, 1964.

APPENDIX

The following data is from experiments conducted by Collins and reported in reference 4.

Table A-1. Calibration of Impact Medium using 57mg Steel Spheres.

Penetration		Measured Velocity		Penetration		Measured Velocity	
in	m	ft/s	m/s	in	m	ft/s	m/s
5.43	0.14	5036	1535	3.05	0.08	2469	753
6.09	0.16	5250	1600	2.78	0.07	2139	652
6.09	0.16	5270	1606	1.85	0.05	1678	511
6.09	0.16	5256	1602	2.52	0.06	2204	672
5.83	0.15	5211	1588	1.99	0.05	1860	567
5.30	0.13	4854	1479	2.25	0.06	1853	565
5.96	0.15	5018	1529	2.25	0.06	2017	615
5.96	0.15	5140	1567	2.78	0.07	2174	663
5.30	0.13	4395	1340	3.05	0.08	2275	693
5.56	0.14	4432	1351	2.78	0.07	2266	691
5.25	0.13	4510	1375	2.52	0.06	2007	612
5.43	0.14	4493	1369	1.85	0.05	1762	537
5.30	0.13	4367	1331	2.52	0.06	2039	621
5.30	0.13	4441	1354	2.52	0.06	2139	652
5.30	0.13	4468	1362	1.33	0.03	1275	389
3.97	0.10	3257	993	0.66	0.02	970	296
4.19	0.11	3330	1015	0.66	0.02	926	282
4.19	0.11	3357	1023	0.93	0.02	1208	368
4.19	0.11	3209	978	0.93	0.02	961	293
3.88	0.10	3304	1007	0.66	0.02	881	269
3.84	0.10	3180	969	0.93	0.02	1127	343
3.84	0.10	3156	962	0.40	0.01	1093	333
3.84	0.10	3156	962	0.40	0.01	709	216
3.84	0.10	3156	962	0.27	0.01	661	201
3.97	0.10	3243	988	0.27	0.01	478	146
4.11	0.01	3263	955	0.13	0.003	371	113
2.52	0.06	2025	617	0.13	0.003	493	150
3.05	0.08	2583	787				
1.72	0.04						

Table A-2. Small Fragment Data: $36\text{mg} \leq m \leq 80\text{mg}$.

mass, M 10^{-5} kg	area, A		penetration, P		measured velocity, v_0	
	10^{-5} ft ²	10^{-6} m ²	in	m	ft/s	m/s
6.10	8.81	8.18	0.93	.024	1333	406
6.60	7.74	7.19	0.40	.010	677	206
7.00	8.00	7.43	0.27	.007	485	14
6.60	7.98	7.41	0.13	.003	299	91
5.80	7.72	7.17	0.13	.003	297	91
3.60	7.22	6.71	0.13	.003	219	67
7.50	9.63	8.95	4.77	.121	5272	1607
8.00	10.96	10.18	4.37	.111	4645	1415
7.00	9.15	8.50	3.31	.084	4816	1468
7.00	8.99	8.35	4.50	.114	5071	1546
7.00	9.11	8.46	4.50	.114	4928	1502
7.00	8.86	8.23	5.03	.128	5220	1591
7.00	9.11	8.46	3.58	.091	4465	1361
7.10	8.89	8.26	4.50	.114	5095	1553
7.10	9.27	8.61	2.39	.061	4665	1422
7.10	9.23	8.57	3.44	.087	4983	1824
7.10	8.93	8.30	3.97	.101	5129	1563
7.10	9.13	8.48	3.44	.087	5289	1612
7.10	9.32	8.66	2.92	.074	5022	1531
7.10	9.52	8.84	3.05	.077	5128	1563
7.20	9.26	8.60	2.78	.071	3958	1206
7.30	9.13	8.48	3.84	.098	4056	1236
7.40	9.63	8.95	2.39	.061	3942	1201
7.40	9.79	9.09	2.52	.064	3951	1204
7.40	9.58	8.90	2.39	.061	4172	1272
7.50	9.06	8.42	2.52	.064	4224	1272
7.50	9.13	8.48	2.39	.061	3991	1216
7.60	9.38	8.71	2.39	.061	3893	1187
7.60	9.56	8.88	3.44	.087	4006	1221
7.60	9.52	8.84	1.99	.051	2774	845
7.80	9.63	8.95	3.05	.077	3165	965
6.90	9.18	8.53	0.80	.020	1756	535
7.00	9.02	8.38	1.99	.051	2120	646
7.00	9.28	8.62	1.46	.037	1920	585
7.00	9.18	8.53	1.85	.047	1987	606
6.90	9.06	8.42	1.99	.051	2232	680
6.90	9.46	8.79	1.99	.051	1925	587
5.80	8.90	8.27	1.46	.037	1861	567
6.50	8.81	8.18	1.19	.030	1311	400
6.60	8.93	8.30	1.19	.030	1292	394
6.70	9.18	8.53	0.13	.003	1292	394
6.80	8.93	8.30	0.27	.007	778	237
6.80	8.82	8.19	0.40	.010	893	272

Table A-2. Small Fragment Data: $36\text{mg} \leq m \leq 80\text{mg}$ (continued)

6.90	9.23	8.57	1.19	.030	1690	515
6.90	9.05	8.41	0.93	.024	1577	481
6.90	9.59	8.91	1.46	.037	2093	638
6.70	8.63	8.02	0.13	.003	466	142
6.70	8.83	8.20	0.27	.007	515	157
6.70	8.73	8.11	0.13	.003	431	131
6.80	8.53	7.92	0.13	.003	539	164

Table A-3. Calibration of Impact Medium using 700mg Steel Spheres.

	Penetration		Measured Velocity			Penetration		Measured Velocity	
	in	m	ft/s	m/s		in	m	ft/s	m/s
m=700mg									
	6.76	0.17	2043	623		14.57	0.37	4306	1312
	7.02	0.18	2024	617		16.03	0.41	4274	1303
	6.49	0.16	2020	616		15.77	0.40	4663	1421
	6.23	0.16	1860	567		17.89	0.45	4780	1457
	8.35	0.21	2485	757		16.30	0.41	4925	1501
	8.75	0.22	1976	602		17.09	0.43	4892	1491
	8.61	0.22	1946	593		19.21	0.49	4950	1509
	10.33	0.26	2210	674		17.75	0.45	4950	1509
	7.02	0.18	2076	633		19.21	0.49	5079	1548
	6.76	0.17	2042	622		19.48	0.50	5074	1546
	6.09	0.15	1962	598		14.97	0.38	4468	1362
	8.88	0.23	2025	616		18.95	0.48	5115	1559
	2.12	0.05	997	298		17.62	0.45	5139	1566
	1.85	0.05	885	270		17.62	0.45	5018	1529
	2.39	0.06	988	301		18.15	0.46	5068	1545
	0.80	0.02	621	189		16.30	0.41	5145	1568
	1.85	0.05	847	258		16.56	0.42	4289	1307
	0.13	0.003	250	76		18.15	0.46	4135	1260
	2.78	0.07	1146	349		13.91	0.35	3838	1170
	1.59	0.04	624	190		16.83	0.43	3868	1179
	0.66	0.02	534	163		15.50	0.39	4070	1240
	1.19	0.03	569	173		15.63	0.40	4160	1268
	1.72	0.04	809	247		15.11	0.38	4155	1266
	2.25	0.06	975	297		14.71	0.37	4037	1230
	0.66	0.02	571	174		13.91	0.35	4001	1219
	2.92	0.07	1150	351		14.71	0.37	4004	1220
	0.93	0.02	711	217		14.97	0.38	3994	1217
	0.93	0.02	647	197		14.44	0.37	3246	989
	2.25	0.06	896	273		14.70	0.37	3211	979
	1.33	0.03	764	233		10.87	0.28	2959	902
	0.80	0.02	507	155		14.57	0.37	3131	954
669 ≤ m < 700mg						10.87	0.28	3057	932
	12.06	0.31	3034	925		12.06	0.31	3106	947
	10.33	0.26	3025	922		11.79	0.30	2990	911
	9.67	0.25	2282	696		10.33	0.26	1961	902

Table A-4. Calibration of Impact Medium using 1025mg Steel Spheres.

Penetration		Measured Velocity		Penetration		Measured Velocity	
in	m	ft/s	m/s	in	m	ft/s	m/s
16.16	0.41	4426	1349	19.48	0.50	5993	1827
13.38	0.34	3452	1052	18.68	0.47	5628	1715
15.11	0.38	4062	1238	20.14	0.51	6240	1902
13.38	0.34	3528	1075	19.48	0.50	6224	1897
14.05	0.36	3553	1083	20.01	0.51	6162	1878
13.65	0.35	3473	1059	17.09	0.43	5165	1574
12.32	0.31	3196	974	20.27	0.52	6227	1898
15.63	0.40	4075	1242	19.74	0.50	6152	1875
15.50	0.39	4033	1229	19.74	0.50	6259	1908
13.12	0.33	3371	1027	18.82	0.48	5481	1671
11.00	0.28	2855	870	16.83	0.43	4609	1405
11.93	0.30	3063	934	18.82	0.48	5370	1637
14.44	0.37	3990	1216	19.48	0.50	5303	1616
15.50	0.39	4220	1286	17.09	0.43	4761	1451
13.12	0.33	3460	1055	17.09	0.43	4805	1464
8.75	0.22	2307	703	18.68	0.47	5348	1630
10.33	0.26	2869	874	18.15	0.46	5291	1613
11.26	0.29	2993	912	18.82	0.48	4802	1464
12.06	0.31	3161	963	17.62	0.45	5244	1598
11.26	0.29	2962	903	18.42	0.47	4754	1449
11.39	0.29	2979	908	18.28	0.46	5052	1540
10.87	0.28	2908	886	17.89	0.45	5022	1531
10.73	0.27	2890	881	17.62	0.45	5085	1550
15.63	0.40	4375	1333	18.28	0.46	5092	1552
12.99	0.33	3670	1119	17.09	0.43	4790	1460
13.51	0.34	3415	1041				

Table A-5. Calibration of Impact Medium using 1002mg to 1059mg Steel Spheres.

Penetration		Measured Velocity		Penetration		Measured Velocity	
in	m	ft/s	m/s	in	m	ft/s	m/s
15.45	0.39	3708	1130	7.29	0.19	1993	607
16.30	0.41	4516	1376	7.29	0.19	1990	607
16.03	0.41	4321	1317	7.29	0.19	2063	629
13.51	0.34	4412	1345	7.29	0.19	1981	604
15.77	0.40	3579	1091	7.29	0.19	1986	605
12.85	0.33	3404	1037	7.16	0.18	2005	611
14.97	0.38	4004	1220	2.78	0.07	966	294
14.05	0.36	3656	1114	2.78	0.07	931	284
15.11	0.38	3927	1197	1.46	0.04	592	180
15.11	0.38	3482	1061	2.39	0.06	749	228
13.65	0.35	3440	1048	1.99	0.05	834	254
14.05	0.36	3590	1094	3.31	0.08	1145	349
14.05	0.36	3734	1138	3.05	0.08	1161	354
12.59	0.32	3524	1074	3.05	0.08	1145	349
13.65	0.35	3720	1134	2.52	0.06	922	281
14.57	0.37	3943	1202	2.52	0.06	925	282
15.50	0.39	4235	1291	1.99	0.05	788	240
8.61	0.22	2218	676	0.80	0.02	771	235
7.29	0.19	1998	609	1.85	0.05	424	129
7.55	0.19	1989	606	0.80	0.02	499	152
7.29	0.19	2049	625	1.72	0.04	721	220
7.55	0.19	2046	624	0.66	0.02	481	147
19.35	0.49	5838	1779	1.19	0.03	616	188
20.01	0.51	6180	1884	1.72	0.04	714	218
				0.13	0.00	396	121
				1.72	0.04	680	207

Table A-6. Fragment Area and Mass Data.

Mass, M	Area, A		Mass, M	Area, A	
	10^{-5} ft ²	10^{-6} m ²		10^{-5} kg	10^{-5} ft ²
8.10	9.83	9.13	8.50	10.31	9.58
9.10	9.42	8.75	8.50	9.58	8.86
9.20	9.60	8.92	8.50	9.68	8.99
9.20	9.77	9.08	8.50	9.48	8.81
9.20	9.67	8.98	8.70	10.00	9.29
9.20	9.68	8.99	6.10	8.81	8.18
9.20	9.42	8.75	6.60	7.74	7.19
9.30	9.72	9.03	7.00	8.00	7.43
9.80	9.46	8.79	6.60	7.98	7.41
9.80	9.78	9.09	5.80	7.72	7.17
9.80	10.16	9.44	3.60	7.22	6.71
9.80	9.71	9.02	7.50	9.63	8.95
10.60	10.65	9.89	8.00	10.96	10.18
10.70	10.84	10.07	8.10	9.56	8.88
11.20	11.17	10.38	8.40	10.25	9.52
14.20	12.24	11.37	9.20	9.99	9.28
8.70	9.22	8.56	9.90	9.73	9.04
8.80	8.91	8.28	10.00	10.69	9.93
8.80	8.54	7.93	10.30	9.23	8.57
8.80	8.22	7.64	10.30	10.55	9.80
8.80	8.76	8.14	10.40	10.70	9.94
8.90	8.47	7.87	10.50	10.47	9.73
9.00	8.76	8.14	10.50	10.81	10.04
14.80	12.35	11.47	10.60	10.68	9.92
15.00	12.12	11.26	10.90	10.58	9.83
15.10	11.55	10.73	11.00	11.00	10.22
15.30	10.92	10.14	11.00	10.21	9.48
16.80	12.98	12.06	11.10	10.98	10.20
17.30	12.71	11.81	11.20	10.59	9.84
17.40	12.31	11.44	11.20	11.12	10.33
17.80	12.73	11.83	11.30	10.66	9.90
18.50	12.71	11.81	11.50	11.05	10.26

Table A-6. Fragment Area and Mass Data (continued).

Mass, M		Area, A		Mass, M		Area, A	
10 ⁻⁵ kg	10 ⁻⁵ ft ²	10 ⁻⁶ m ²	10 ⁻⁵ ft ²	10 ⁻⁵ kg	10 ⁻⁵ ft ²	10 ⁻⁶ m ²	10 ⁻⁶ m ²
20.50	14.40	13.38	11.50	11.50	11.31	10.51	10.51
8.20	9.79	9.09	11.80	11.80	11.82	10.98	10.98
8.30	10.14	9.42	11.80	11.80	11.64	10.81	10.81
8.40	9.96	9.25	11.80	11.80	11.72	10.89	10.89
8.40	9.38	8.71	11.80	11.80	11.65	10.82	10.82
11.90	11.65	10.82	7.40	7.40	9.63	8.95	8.95
11.90	11.32	10.52	7.40	7.40	9.79	9.09	9.09
11.90	11.61	10.78	7.40	7.40	9.58	8.90	8.90
12.50	11.59	10.77	7.50	7.50	9.06	8.42	8.42
12.80	11.54	10.72	7.50	7.50	9.13	8.48	8.48
13.00	11.64	10.81	7.60	7.60	9.38	8.71	8.71
13.00	11.74	10.91	7.60	7.60	9.56	8.88	8.88
13.00	11.46	10.65	7.60	7.60	9.52	8.84	8.84
13.00	11.47	10.65	7.80	7.80	9.63	8.95	8.95
8.10	9.56	8.88	8.20	8.20	9.63	8.95	8.95
8.40	10.25	9.52	8.70	8.70	10.91	10.13	10.13
9.20	9.94	9.23	10.40	10.40	11.44	10.63	10.63
9.20	9.99	9.28	12.30	12.30	15.48	14.38	14.38
9.10	9.93	9.22	12.60	12.60	11.87	11.03	11.03
9.90	10.69	9.93	13.60	13.60	12.60	11.70	11.70
9.90	9.73	9.04	13.80	13.80	14.72	13.67	13.67
10.00	10.69	9.93	14.60	14.60	13.99	13.00	13.00
10.30	9.23	8.57	6.90	6.90	9.18	8.53	8.53
10.30	10.55	9.80	7.00	7.00	9.02	8.38	8.38
10.40	10.70	9.94	15.00	15.00	13.36	12.41	12.41
10.50	10.75	9.99	15.60	15.60	14.87	13.81	13.81
10.50	10.47	9.73	7.00	7.00	9.28	8.62	8.62
10.50	10.81	10.04	7.00	7.00	9.18	8.53	8.53
10.60	10.68	9.92	6.90	6.90	9.06	8.42	8.42
7.00	9.15	8.50	6.90	6.90	9.46	8.79	8.79
7.00	8.99	8.35	5.80	5.80	8.90	8.27	8.27

Table A-6. Fragment Area and Mass Data (continued).

Mass, M 10 ⁻⁵ kg	Area, A		Mass, M 10 ⁻⁵ kg	Area, A	
	10 ⁻⁵ ft ²	10 ⁻⁶ m ²		10 ⁻⁵ ft ²	10 ⁻⁶ m ²
7.00	9.11	8.46	6.50	8.81	8.18
7.00	8.86	8.23	6.60	8.93	8.30
7.00	9.11	8.46	6.70	9.18	8.53
7.10	8.89	8.26	6.80	8.93	8.30
7.10	9.27	8.61	6.80	8.82	8.19
7.10	9.23	8.57	6.90	9.23	8.57
7.10	8.93	9.13	6.90	9.05	8.41
7.10	9.32	8.66	6.70	8.63	8.02
7.10	9.52	8.84	6.70	8.83	8.20
7.20	9.26	8.60	6.70	8.73	8.11
7.30	9.13	8.48	6.70	8.63	8.02
			6.80	8.53	7.42

No of Copies	<u>Organization</u>	No of Copies	<u>Organization</u>
(Unclass., unlimited) 12	Administrator	1	Commander
(Unclass., limited) 2	Defense Technical Info Center		US Army Missile Command
(Classified) 2	ATTN: DTIC-DDA Cameron Station Alexandria, VA 22304-6145		ATTN: AMSMI-RD-CS-R (DOC) Redstone Arsenal, AL 35898-5010
1	HQDA (SARD-TR) WASH DC 20310-0001	1	Commander
1	Commander		US Army Tank Automotive Command
	US Army Materiel Command		ATTN: AMSTA-TSL (Technical Library Warren, MI 48397-5000
	ATTN: AMCDRA-ST 5001 Eisenhower Avenue Alexandria, VA 22333-0001	1	Director
1	Commander		US Army TRADOC Analysis Command
	US Army Laboratory Command		ATTN: ATAA-SL White Sands Missile Range, NM 88002-
	ATTN: AMSLC-DL Adelphi, MD 20783-1145	(Class. only) 1	Commandant
2	Commander		US Army Infantry School
	Armament RD&E Center		ATTN: ATSH-CD (Security Mgr.) Fort Benning, GA 31905-5660
	US Army AMCCOM	(Unclass. only) 1	Commandant
	ATTN: SMCAR-MSI Picatinny Arsenal, NJ 07806-5000		US Army Infantry School
2	Commander		ATTN: ATSH-CD-CSO-OR Fort Benning, GA 31905-5660
	Armament RD&E Center	(Class. only) 1	The Rand Corporation
	US Army AMCCOM		P.O. Box 2138
	ATTN: SMCAR-TDC Picatinny Arsenal, NJ 07806-5000		Santa Monica, CA 90401-2138
1	Director	1	Air Force Armament Laboratory
	Benet Weapons Laboratory		ATTN: AFATL/DLODL
	Armament RD&E Center		Eglin AFB, FL 32542-5000
	US Army AMCCOM		<u>Aberdeen Proving Ground</u>
	ATTN: SMCAR-LCB-TL Watervliet, NY 12189-4050		Dir, USAMSAA
1	Commander		ATTN: AMXSY-D AMXSY-MP, H. Coher
	US Army Armament, Munitions and Chemical Command		Cdr, USATECOM
	ATTN: SMCAR-ESP-L Rock Island, IL 61299-5000		ATTN: AMSTE-TO-F
1	Commander		Cdr, CRDEC, AMCCOM
	US Army Aviation Systems Command		ATTN: SMCCR-RSP-A SMCCR-MU SMCCR-MSI
	ATTN: AMSAV-DACL 4300 Goodfellow Blvd. St. Louis, MO 63120-1798		Dir, VLAMO
1	Director		ATTN: AMSLC-VL-D
	US Army Aviation Research and Technology Activity		
	Ames Research Center		
	Moffett Field, CA 94035-1099		

USER EVALUATION SHEET/CHANGE OF ADDRESS

This laboratory undertakes a continuing effort to improve the quality of the reports it publishes. Your comments/answers below will aid us in our efforts.

1. Does this report satisfy a need? (Comment on purpose, related project, or other area of interest for which the report will be used.) _____

2. How, specifically, is the report being used? (Information source, design data, procedure, source of ideas, etc.) _____

3. Has the information in this report led to any quantitative savings as far as man-hours or dollars saved, operating costs avoided, or efficiencies achieved, etc? If so, please elaborate. _____

4. General Comments. What do you think should be changed to improve future reports? (Indicate changes to organization, technical content, format, etc.) _____

BRL Report Number _____ Division Symbol _____

Check here if desire to be removed from distribution list. _____

Check here for address change. _____

Current address: Organization _____
Address _____

-----FOLD AND TAPE CLOSED-----

Director
U.S. Army Ballistic Research Laboratory
ATTN: SLCBR-DD-T (NEI)
Aberdeen Proving Ground, MD 21005-5066

OFFICIAL BUSINESS



NO POSTAGE
NECESSARY
IF MAILED
IN THE
UNITED STATES

BUSINESS REPLY LABEL
FIRST CLASS PERMIT NO 12062 WASHINGTON D C.

POSTAGE WILL BE PAID BY DEPARTMENT OF THE ARMY



Director
U.S. Army Ballistic Research Laboratory
ATTN: SLCBR-DD-T (NEI)
Aberdeen Proving Ground, MD 21005-9989